

Dynamical crystal creation with polar molecules or Rydberg atoms in optical lattices

This content has been downloaded from IOPscience. Please scroll down to see the full text.

2010 New J. Phys. 12 103044

(<http://iopscience.iop.org/1367-2630/12/10/103044>)

View [the table of contents for this issue](#), or go to the [journal homepage](#) for more

Download details:

IP Address: 92.22.48.247

This content was downloaded on 03/11/2013 at 13:15

Please note that [terms and conditions apply](#).

Corrigendum

Dynamical crystal creation with polar molecules or Rydberg atoms in optical lattices

J Schachenmayer, I Lesanovsky, A Micheli and A J Daley 2010 *New J. Phys.*
[12 103044](#)

New Journal of Physics **13** (2011) 059503 (3pp)

Received 17 December 2010

Published 19 May 2011

Online at <http://www.njp.org/>

doi:10.1088/1367-2630/13/5/059503

In the paper [1], the dependence of the matrix elements in equation (10) on the dipole-operator elements was incorrectly oversimplified. This led to an oversimplified discussion of how the experimental parameters should be chosen in order to implement the model with polar molecules, and made the quantities plotted in figure 12 somewhat misleading. This discussion is corrected below. We note that the optimal parameter regime for experiments is essentially the same as that indicated in the original paper, and that the deviation of the final Hamiltonian parameters calculated in the original paper is very small in this regime. No other part of the published paper or conclusions are affected in any way.

The correct expression for V_d in equation (10) is

$$\hat{V}_d \equiv \begin{pmatrix} v_{\alpha\alpha}^{\alpha\alpha} & 0 & 0 & 0 \\ 0 & v_{\alpha\beta}^{\alpha\beta} & v_{\alpha\beta}^{\beta\alpha} & 0 \\ 0 & v_{\alpha\beta}^{\beta\alpha} & v_{\alpha\beta}^{\alpha\beta} & 0 \\ 0 & 0 & 0 & v_{\beta\beta}^{\beta\beta} \end{pmatrix},$$

where in the rotating wave approximation, the non-vanishing elements of \hat{V}_d are related to the bare single-particle dipole-operator elements $d_{ij} \equiv \langle i | \hat{d}_k^z | j \rangle_{dc}$ by

$$v_{\alpha\alpha}^{\alpha\alpha} = (\cos^2(\theta/2)d_{11} + \sin^2(\theta/2)d_{22})^2 + 2 \sin^2(\theta/2) \cos^2(\theta/2)d_{12}^2, \quad (1)$$

$$v_{\alpha\beta}^{\alpha\beta} = d_{00}(\cos^2(\theta/2)d_{11} + \sin^2(\theta/2)d_{22}), \quad (2)$$

$$v_{\alpha\beta}^{\beta\alpha} = \cos^2(\theta/2)d_{10}^2 + \sin^2(\theta/2)d_{02}^2, \quad (3)$$

$$v_{\beta\beta}^{\beta\beta} = d_{00}^2. \quad (4)$$

To find optimal values of the microwave dressing angle θ and the static field strength E_{dc} so that the desired Hamiltonian (equation (1)) is realized with as small an error as possible,

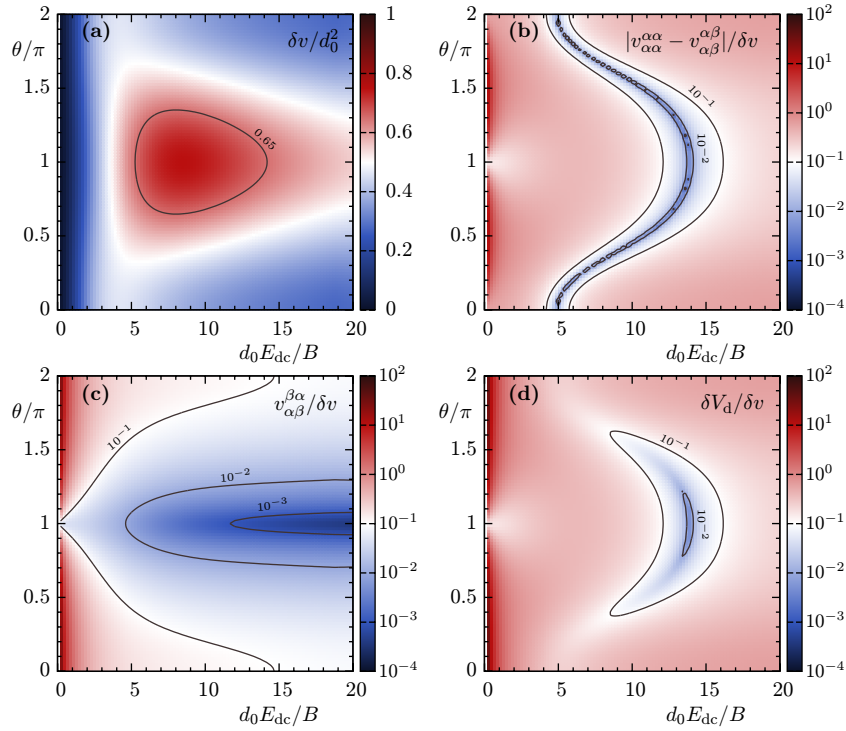


Figure 1. Matrix elements of the dipole–dipole interaction matrix \hat{V}_d in static and microwave fields, E_{dc} and $E_2^z(t)$. (a) Interaction strength for the strongly interacting state, δv (in units of d_0^2). (b) The ratio $|v_{\alpha\alpha}^{\alpha\alpha} - v_{\alpha\beta}^{\alpha\beta}|/\delta v$ of the diagonal element of \hat{V}_d and (c) of the off-diagonal element, $v_{\alpha\beta}^{\beta\alpha}/\delta v$, as a function of the static-field strength $d_0 E_{dc}/B$ and the microwave-dressing angle θ on a logarithmic scale. (d) The relative deviation, $\delta V_d/\delta v$, of the induced dipole–dipole coupling with respect to the model interaction as a function of $d_0 E_{dc}/B$ and θ on a logarithmic scale. The solid lines show contours of constant value.

we must now consider the matrix elements V_d separately, and not just the dipole operator elements, as was done in figure 12 of the original paper. Although from equation (3) we see that there is no parameter choice where $v_{\alpha\beta}^{\beta\alpha}$ is exactly zero, we can find regimes where the model is implemented up to very small errors. At this point we note that subtracting a multiple of the identity from V_d amounts to an overall shift of the zero of energy, and thus we can equivalently write

$$\hat{V}'_d \equiv \begin{pmatrix} v_{\alpha\alpha}^{\alpha\alpha} - v_{\alpha\beta}^{\alpha\beta} & 0 & 0 & 0 \\ 0 & 0 & v_{\alpha\beta}^{\beta\alpha} & 0 \\ 0 & v_{\alpha\beta}^{\beta\alpha} & 0 & 0 \\ 0 & 0 & 0 & \delta v \end{pmatrix},$$

where $\delta v \equiv v_{\beta\beta}^{\beta\beta} - v_{\alpha\beta}^{\alpha\beta}$.

In figure 1, we plot the matrix elements δv , $|v_{\alpha\alpha}^{\alpha\alpha} - v_{\alpha\beta}^{\alpha\beta}|$ and $v_{\alpha\beta}^{\beta\alpha}$ as a function of the microwave field angle θ and the electric field strengths up to $E_{dc} = 20d_0/B$. In figure 1(a), we show the magnitude of the interaction energy for the strongly interacting state, δv . Figures 1(b)

and (c) show the ratio of the other interaction matrix elements to δv , i.e. $|v_{\alpha\alpha}^{\alpha\alpha} - v_{\alpha\beta}^{\alpha\beta}|/\delta v$ and $|v_{\alpha\beta}^{\beta\alpha}|/\delta v$. In figure 1(d), we plot the (normalized) total deviation from an exact implementation of the Hamiltonian (equation (1)). This is quantified as $\delta V_d/\delta v$, given by

$$\delta V_d \equiv \|\hat{V}'_d - \delta v |\beta\rangle_k \langle\beta|_l \langle\beta|_k \langle\beta|_l\| = \sqrt{(v_{\alpha\alpha}^{\alpha\alpha} - v_{\alpha\beta}^{\alpha\beta})^2 + 2(v_{\alpha\beta}^{\beta\alpha})^2}. \quad (5)$$

We find that for field strengths $E_{dc} \sim 14B/d_0$, fine-tuning the microwave field at $\theta \sim 0.9\pi$ makes it possible to obtain deviations $\delta V_d \sim 10^{-3}\delta v$, while the interaction strength for the strongly interacting state is $\delta v \approx 0.65d_0^2$ (see the contour line in 1(a)). Thus within small errors (similar to those in the parameter regime quoted in the original paper) we obtain the model interaction with a typical timescale of $V_{dd} \equiv 2\delta v V_{dd}^{(1)} \approx \delta v/4\pi\epsilon_0 a^3 \approx 10\hbar$ kHz for typical parameters ($a = 400$ nm, $d_0 = 0.8$ Debye). An alternative approach using circularly polarized coupling fields is also possible, which can give rise to an implementation of the model for appropriately tuned parameters [2].

We note again that this parameter regime is essentially the same as that quoted in the original paper, and that no other conclusions of the paper are affected by this modification. We would like to thank Alexey Gorshkov for bringing this error in the original paper to our attention, and for additional further discussions related to the experimental implementation.

References

- [1] Schachenmayer J, Lesanovsky I, Micheli A and Daley A J 2010 *New J. Phys.* **12** 103044
- [2] Gorshkov A *et al* 2011 in preparation

Dynamical crystal creation with polar molecules or Rydberg atoms in optical lattices

J Schachenmayer^{1,3}, I Lesanovsky², A Micheli¹ and A J Daley¹

¹ Institute for Theoretical Physics, University of Innsbruck, and Institute for Quantum Optics and Quantum Information of the Austrian Academy of Sciences, A-6020 Innsbruck, Austria

² School of Physics and Astronomy, The University of Nottingham, University Park, Nottingham NG7 2RD, UK

E-mail: johannes.schachenmayer@uibk.ac.at

New Journal of Physics **12** (2010) 103044 (28pp)

Received 30 March 2010

Published 29 October 2010

Online at <http://www.njp.org/>

doi:10.1088/1367-2630/12/10/103044

Abstract. We investigate the dynamical formation of crystalline states with systems of polar molecules or Rydberg atoms loaded into a deep optical lattice. External fields in these systems can be used to couple the atoms or molecules between two internal states: one that is weakly interacting and one that exhibits a strong dipole–dipole interaction. By appropriate time variation of the external fields, we show that it is possible to produce crystalline states of the strongly interacting states with high filling fractions chosen via the parameters of the coupling. We study the coherent dynamics of this process in one dimension (1D) using a modified form of the time-evolving block decimation (TEBD) algorithm, and obtain crystalline states for system sizes and parameters corresponding to realistic experimental configurations. For polar molecules these crystalline states will be long-lived, assisting in a characterization of the state via the measurement of correlation functions. We also show that as the coupling strength increases in the model, the crystalline order is broken. This is characterized in 1D by a change in density–density correlation functions, which decay to a constant in the crystalline regime, but show different regions of exponential and algebraic decay for larger coupling strengths.

³ Author to whom any correspondence should be addressed.

Contents

1. Introduction and overview	2
2. The system	4
2.1. Polar molecules	4
2.2. Neutral atoms coupled to Rydberg states	5
2.3. The effective model	6
3. Numerical method	6
4. Ground states of the effective model	7
5. Dynamical creation of crystalline states	13
5.1. Time-dependent state preparation	13
5.2. Comparison with experimental parameters	17
6. Physical implementations of a long-range spin model	18
6.1. Polar molecules in an optical lattice	18
6.2. Neutral atoms coupled to Rydberg states	22
7. Conclusion and outlook	26
Acknowledgments	26
References	26

1. Introduction and overview

Recent experimental progress in controlled excitation of Rydberg atoms from cold gases [1]–[6] and in the production of ultracold polar molecules [7] has opened new opportunities for the study of systems with dipole–dipole interactions. Key features of these systems include the ability to control these interactions by varying the external fields, as well as the strong dependence of the interaction strength on the internal state of the atoms or molecule. An important example of this dependence is the Rydberg blockade mechanism [8, 9] in which an atom in an excited Rydberg state can prevent nearby atoms from being excited to Rydberg states, because the strong interaction between the two excited atoms makes subsequent excitations non-resonant. This mechanism has been recently demonstrated in experiments [10, 11], and has important potential applications in the production of fast quantum gates with two or several neutral atoms [8, 9, 12, 13]. Moreover, the blockade produces rich and intriguing collective dynamics when atoms in a dense gas are excited to Rydberg states [1]–[6], [14]–[16]. This cooperative behaviour is manifest in a suppression of the proportion of excited atoms with increasing density (due to the presence of more atoms within the blockade radius), and also in an enhanced laser coupling to collective Rydberg excitations.

In the context of Rydberg atoms, there has been a lot of interest in the possible production of crystalline states, where a small fraction of atoms in excited Rydberg states arrange themselves in a regular array [17]–[20]. In particular, when ground and excited states are coupled by a laser field, the resulting effective models correspond to crystalline states in the limit of weak coupling, with the fraction of excited atoms determined by a competition between the interaction energy and the detuning of the laser field from the atomic transition.

Motivated by this experimental and theoretical progress, we consider here a collection of either polar molecules or neutral atoms loaded into a deep optical lattice, e.g. with one particle

per site. We assume that tunnelling in the lattice is negligible on the timescale of the experiment. Using dressed rotational states for the polar molecules or Rydberg states for the atoms we show how a microscopic model can be realized where two internal states of the particles are accessed, one of which exhibits a large dipole–dipole interaction, while the other is weakly interacting. We show that this system allows the realization of crystalline formations in the internal states, with a periodicity related to the lattice period by a rational fraction. The regularity of the system makes it possible to realize crystals with high filling factors of strongly interacting states. In addition, the use of polar molecules makes it possible for the crystalline states to be long-lived, aiding in the measurement of characteristic correlation functions. We show that in a one-dimensional (1D) tube, increasing the coupling strength between the internal states at a fixed detuning will break the crystalline order. This is characterized in 1D by a change in the density–density correlation (DDC) functions, which decay to a constant in the crystalline regime, but show different regions of exponential and algebraic decay for larger coupling strengths.

We study in detail the dynamical preparation of states with crystalline order of different periodicities in the internal states by an appropriate time variation of microwave or laser couplings. As was shown in previous studies for Rydberg atoms in an optical lattice modelled by nearest-neighbour interactions [14]–[16], it is not possible to produce crystalline states simply by switching on the coupling field. Instead, this is made possible using an adiabatic variation of the parameters in the effective model. Using an extended version of the time-evolving block decimation (TEBD) algorithm [21, 22], we calculate the coherent time-dependent many-body dynamics of the excitations. We show that for system sizes and parameters corresponding to realistic experimental configurations with either polar molecules or Rydberg atoms, we obtain fidelities $>99\%$ compared with the ideal target states, i.e. the ground states of the effective model. While the fidelity could be reduced by incoherent processes, e.g. decay of excited states, we estimate that these rates are small and that the basic structure of the crystalline state will be robust. Note that the time-dependent preparation of crystalline phases here follows the same philosophy as that for the production of Rydberg crystals in [20]. Focusing on the case of atoms or molecules initially trapped in a lattice, we concentrate here on the case with a high proportion of particles in the strongly interacting case. This is in contrast to [20], which treats the case of a dilute gas of Rydberg excitations that is more relevant for a frozen Rydberg gas not trapped in a lattice. Our study of the correlation functions in the crystalline and non-crystalline phases is, however, also relevant for the case of [20].

The remainder of the paper is organized as follows: in section 2, we introduce the effective long-range spin model that describes both the Rydberg atoms and the polar molecules in appropriate parameter regimes. Then we briefly discuss in section 3 extensions to the TEBD algorithm that we use to study the model. In section 4, we analyse the ground states of this effective model and identify a target state of our time-dependent excitation process. The ground states are characterized as belonging to different quantum phases via the characteristic behaviour of DDC functions. In section 5, we discuss a scheme to prepare crystalline states with high fidelity by appropriate time dependence of the external coupling field parameters. In section 6, details of two different physical realizations of the effective model, with polar molecules (section 6.1) and Rydberg atoms (section 6.2), are provided. Finally, section 7 provides the conclusion and outlook.

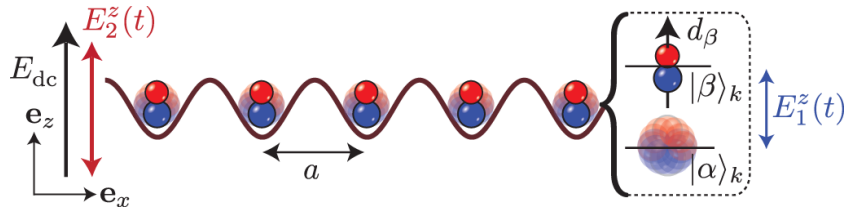


Figure 1. Schematic illustration of a system of polar molecules loaded into subsequent sites of a 1D optical lattice with site separation a . The molecules are aligned by a static electric field in the \mathbf{e}_z -direction, E_{dc} , and exposed to two time-dependent microwave fields $E_1^z(t)$ and $E_2^z(t)$, both linearly polarized along the z -axis.

2. The system

We consider particles loaded into an optical lattice in a regime where the lattice is sufficiently deep so that tunnelling can be neglected on the timescale of the experiment. We assume that the particles have two internal states, one of which exhibits a strong dipole–dipole interaction, while the other is weakly interacting. This can be realized for realistic experimental parameters with either

1. *Polar molecules* in an external electric field, where a microwave coupling of rotational states can give rise to dressed states with different dipole–dipole interactions, or
2. *Neutral atoms* in an external electric field coupled via a laser to excited Rydberg states, which in contrast to the ground states exhibit a strong dipole–dipole interaction.

Below we summarize the key points of each of these implementations. Further details of polar molecules and neutral atoms coupled to excited Rydberg states are given in section 6.1 and section 6.2, respectively.

2.1. Polar molecules

Polar molecules in their electronic-vibrational ground-state manifold possess a number of features that make them appealing to design and implement specific spin models. In addition to their electric structure, allowing e.g. for optical trapping, they have a rich internal (rotational) symmetry, with level spacings in the GHz regime, and negligible decoherence. They possess a permanent dipole moment d_0 (typically of the order of a few Debyes [23, 24]) along the internuclear axis, which makes it possible to strongly couple their rotational excitations via static and microwave fields and gives rise to dipole–dipole interactions between different molecules.

We consider a 1D optical lattice (lattice spacing a) along the \mathbf{e}_x -axis with one polar molecule trapped at each lattice site in the lowest vibrational state $\phi_k(\mathbf{x})$ (see figure 1), which can be realized either by loading an insulator state of polar molecules or by beginning deep in a Mott insulator state with two atoms per site and associating them to form polar molecules [25]. Without external fields, the rotational states of the molecules do not possess a net dipole moment. However, finite dipole moments along the z -axis in the rotational states can be induced by applying a static external electric field E_{dc} in that direction. The key idea of our

implementation is that a suitable choice of $E_2^z(t)$ makes it possible to cancel the induced dipole moment in one of the dressed states, and we denote the complete state of an atom in this dressed state at site k as $|\alpha\rangle_k$. The single molecule ground state, which obtains a strong dipole moment from the static electric field, is denoted as $|\beta\rangle_k$. In the case when E_{dc} and $E_2^z(t)$ are properly tuned, two molecules at distinct sites k and l that are in the states $|\beta\rangle_k$ and $|\beta\rangle_l$ lead to an energy shift due to the dipole–dipole interaction potential of $V_{dd}/|k-l|^3$. In section 6.1, we give example experimental parameters showing that an energy shift $V_{dd} \approx 0.7d_0^2/4\pi\epsilon_0a^3 \approx 10\hbar$ kHz can be achieved. Note that we can therefore assume that the molecules remain in their motional ground state, since the band separation (trapping frequency) ω_T is typically of the order of many tens of kHz up to 100 kHz in a realistic scenario. Finally, the states $|\beta\rangle_k$ and $|\alpha\rangle_k$ on all sites k are coupled by a weak microwave field $E_1^z(t)$ with Rabi frequency Ω and detuning δ , which gives rise to the effective microscopic many-body model that is described in section 2.3 below.

2.2. Neutral atoms coupled to Rydberg states

Neutral atoms in an external electric field exhibit strong dipole–dipole interactions when in certain Rydberg states with relatively large principal quantum number. For alkali atoms in states with principal quantum number $n = 17$, it is possible to obtain a dipole moment of more than one kiloDebye (see section 6.2 for details). By finding isolated Rydberg states, the internal dynamics of each atom can be reduced to a two-level system, where weakly interacting atoms in the ground state are coupled via a laser to these states with large dipole–dipole interactions.

We assume that either atoms are loaded into a deep optical lattice with tight radial confinement, so that we have one atom per site along a 1D tube, or that we have weak radial confinement and many atoms per site (as occurs, e.g., when an optical lattice is applied along only one direction). In each case, we can assume that the ground-state atoms are confined to a single modefunction at each given lattice site, $\phi_k(\mathbf{x})$. In the case of a single atom per site, this is the Wannier function for the lowest Bloch band, which is analogous to the case of the polar molecules described above. For many atoms per site, interactions can populate higher bands, and $\phi_k(\mathbf{x})$ will depend on the interactions. However, we assume that the timescale for excitation to the Rydberg state is much shorter than timescales corresponding to the atomic motion and that therefore we can neglect population of any modefunction other than the initial modefunction $\phi_k(\mathbf{x})$ for either the ground or Rydberg states. We then assume that we can have at most one excitation per lattice site, which in the case of large single-site populations is made possible by the Rydberg blockade mechanism, when we ensure that the blockade radius is larger than the occupied region at any single lattice site (see section 6.2). This makes it possible to describe the system with an effective spin-1/2 model, assigning a state on each lattice site to the existence or non-existence of an atom in an excited Rydberg state on that site, labelled for site k by the states $|\beta\rangle_k$ and $|\alpha\rangle_k$, respectively.

In comparison with polar molecules, the dipole–dipole interaction of the strongly interacting state for Rydberg atoms is much larger. If we choose a principal quantum number $n = 14$, then $V_{dd} \approx 7\hbar$ GHz (assuming a lattice spacing of $a = 400$ nm, see section 6.2 for more details). This corresponds to much faster experimental timescales. However, the polar molecules are much longer lived than atoms in excited Rydberg states, and open up different opportunities for experimental observation of the crystalline states we discuss here.

2.3. The effective model

In either the polar molecule or neutral atom case, we can derive the same effective microscopic model for the system in a frame rotating with the frequency of the field coupling the two internal states. We assume that at most one particle per site can be in the strongly interacting state, and represent the two possible states (weakly and strongly interacting) at each lattice site as two spin states. We label these states for site k as $\{|\beta\rangle_k, |\alpha\rangle_k\}$, where $|\beta\rangle_k$ is the state exhibiting strong dipole–dipole interactions, and $|\alpha\rangle_k$ the non-interacting state. The Hamiltonian can then be formulated as ($\hbar \equiv 1$)

$$\hat{H} = \Omega \sum_k \hat{\sigma}_k^x - \delta \sum_k \hat{n}_k + \frac{V_{\text{dd}}}{2} \sum_{k \neq m} \frac{\hat{n}_k \hat{n}_m}{|k - m|^3}, \quad (1)$$

with $\hat{n}_k \equiv |\beta\rangle\langle\beta|_k$ being the local ‘number operator’ for the interacting state at site k . The Pauli matrices are defined via $\hat{\sigma}_k^x \equiv |\beta\rangle\langle\alpha|_k + |\alpha\rangle\langle\beta|_k$ and $\hat{\sigma}_k^z \equiv |\beta\rangle\langle\beta|_k - |\alpha\rangle\langle\alpha|_k$, where the latter is related to the number operators via $\hat{n}_k = (\hat{\sigma}_k^z + 1)/2$. Ω denotes the effective Rabi frequency and δ the detuning of the laser, which excites the particles. V_{dd} is the dipole–dipole interaction energy shift between neighbouring sites. Note that we assume the particles remain in the motional states $\phi_k(\mathbf{x})$ and also neglect corrections to the $|k - m|^{-3}$ decay due to the finite width of $\phi_k(\mathbf{x})$ (see section 6 for more details).

Below we will first study the ground-state properties of this model, which will give us target states for the dynamical preparation process. We will then study the time dependence of this system starting from a many-body state where all of the particles are weakly interacting ($\bigotimes_k |\alpha\rangle_k$), and investigate the adiabatic preparation of crystalline states as the parameters are varied.

It is interesting to note that for an infinite system, the Hamiltonian can be written as

$$\hat{H}_S = \Omega \sum_k \hat{\sigma}_k^x + \frac{1}{2}(\zeta(3)V_{\text{dd}} - \delta) \sum_k \hat{\sigma}_k^z + \frac{V_{\text{dd}}}{8} \sum_{k \neq m} \frac{\hat{\sigma}_k^z \hat{\sigma}_m^z}{|k - m|^3} \quad (2)$$

where we have removed constant terms, and $\zeta(3) \equiv \sum_k k^{-3} \approx 1.202$ denotes Apéry’s constant [27]. Note that in the case of $\delta = \zeta(3)V_{\text{dd}}$, the system is equivalent to an Ising model in a transverse field with dipolar interactions. Ground states of this model have also been studied in [28].

3. Numerical method

To calculate the many-body dynamics and ground states of Hamiltonian (1), we make use of the TEBD algorithm as introduced in [21, 22]. This algorithm makes possible the near-exact integration of the Schrödinger equation for 1D lattice and spin Hamiltonians based on a matrix product state ansatz, and has been applied to a range of such Hamiltonians with nearest-neighbour interactions. There are also applications of matrix product state algorithms to dissipative systems [29]–[31], and these methods have been incorporated within density matrix renormalization group algorithms [32, 33]. There is also a strong effort to extend these ideas to higher dimensions [34].

The modification in our work is the extension of these methods to the treatments of finite-range interactions. For the purposes of this study, we include long-range interactions up to an arbitrary distance of l sites, by implementing a routine for swapping site indices in the matrix

product state representation. This adds a computational cost of $\mathcal{O}(l)$ basic operations compared to the standard TEBD calculation. Here we work with finite systems of size N , and always properly represent interactions over the full length of the system, i.e. $l = N - 1$. This method of swapping also allows us to consider periodic boundary conditions for the dipole–dipole interactions. Note that we always perform convergence tests in the matrix product state bond-dimension χ and other numerical parameters⁴. For larger system sizes, swapping sites can become inefficient, in part due to the higher required values of χ . To implement interaction terms over substantially larger distances than in this study, more efficient algorithms should be used, e.g. algorithms involving the use of matrix product operators [36]–[38].

4. Ground states of the effective model

We begin by studying the key ground-state properties of the effective model of Hamiltonian (1). This will allow us to determine in which parameter regimes crystalline order will appear, and to characterize the states that will be the target states of the dynamical preparation process discussed next in section 5.

The Hamiltonian we study here has strong similarities to another model treated in several recent studies, in which the dipole–dipole interactions were replaced with van der Waals interactions arising for certain Rydberg systems [16]–[20]. In [17], it was shown that for $\Omega = 0$ that system reduces to a classical spin model exhibiting a second-order phase transition from a paramagnetic to a crystalline phase at $\delta = 0$, and we observe similar behaviour here. Due to the dipolar long-range character we expect crystalline states with different periodicities of the excitations to the strongly interacting state to appear for $\delta > 0$ and small values of Ω . The detuning plays the role of a chemical potential for strongly interacting states (or external magnetic field in the spin model), and it becomes favourable to excite states with a dipole–dipole interaction on the lattice. However, the long-range interactions will compete energetically with the detuning, leading to crystal periodicities that decrease with increasing δ/V_{dd} . Below we show that as the coupling Ω/V_{dd} is increased, the crystalline order is broken, in favour of a paramagnetic phase in the spin language, with no long-range density–density ordering. These key features of the phase diagram are sketched in figure 2.

We compute the ground state of equation (1) using the TEBD algorithm in several different parameter regimes. As a first step, we look at the total number of particles in a strongly interacting state $|\beta\rangle$,

$$N_\beta \equiv \sum_k^N \langle \hat{n}_k \rangle. \quad (3)$$

In figure 3, we present a plot of N_β for several detunings δ and effective Rabi frequencies Ω . We plot N_β on a grid with spacings $\Delta\delta = 0.125V_{\text{dd}}$ and $\Delta\Omega = 0.025V_{\text{dd}}$.

As expected, for small Ω/V_{dd} there is essentially no occupation of the strongly interacting states in regions with negative detuning, because a state with no $|\beta\rangle_k$ excitations is energetically favoured. In contrast, a positive detuning leads to a reduction of the total energy when occupations of strongly interacting states are added to the system, and in regions with large positive detuning we find states with occupation of $|\beta\rangle_k$ on all lattice sites. In the region in between, we observe varying excitation numbers depending on the choice of parameters. In

⁴ For a more detailed analysis of how errors enter this method, see [35].

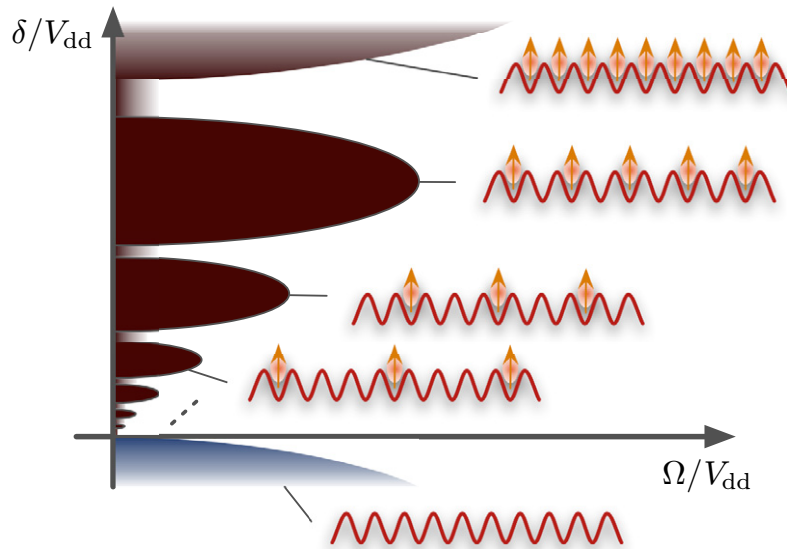


Figure 2. A sketch of the key features of the phase diagram for the system with Hamiltonian (1). For $\delta < 0$ and $\Omega/V_{dd} \ll 1$, the ground state involves all of the atoms in the non-interacting state in order to minimize the interaction energy (marked by the blue lobe). As the detuning $\delta > 0$ is increased, it becomes favourable to add excitations to the system, but this competes with an increasing interaction energy. This competition gives rise to crystalline phases with periodicities determined by this competition (marked by the brown lobes). For large Ω/V_{dd} , the crystalline order is broken, but some particles exist in excited states (white area).

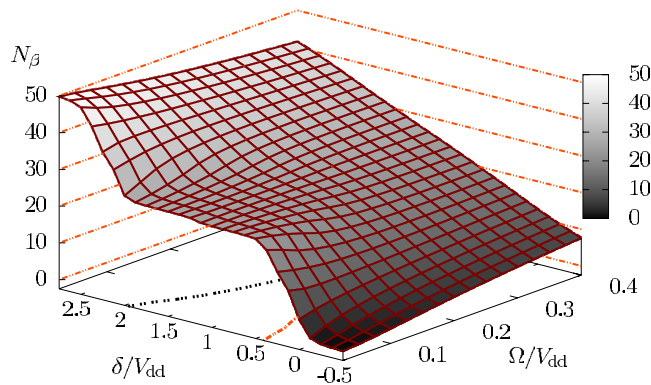


Figure 3. Occupation number of strongly interacting states, N_β , for ground states of the effective model in a 50-site system. The Hamiltonian is given through equation (1) and open boundary conditions are assumed. Results are shown for several values of detuning δ and Rabi frequency Ω , and plateaus of zero, half and full filling of the lattice are clearly visible for $\Omega \lesssim 0.1 V_{dd}$ (see text). The contours of $N_\beta = 23$ and $N_\beta = 27$ are drawn as lines on the δ - Ω plane.

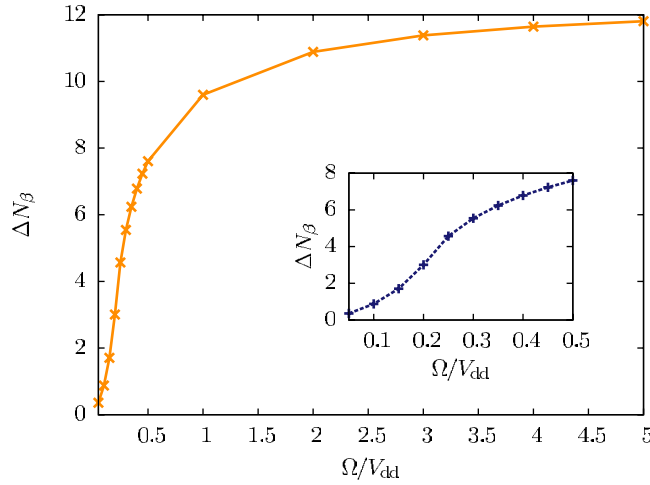


Figure 4. Fluctuation of the total occupation number of the strongly interacting state in a 50-site system with open boundary conditions as a function of Ω for $\delta = 1.1V_{\text{dd}}$. The inset shows a zoom into the region $0.05V_{\text{dd}} \leq \Omega \leq 0.5V_{\text{dd}}$.

particular, there is a large plateau in the region $0.5V_{\text{dd}} \lesssim \delta \lesssim 2V_{\text{dd}}$ and $\Omega \lesssim 0.1V_{\text{dd}}$, in which N_{β} remains close to $N/2 = 25$. In the plot the contours of fillings slightly smaller ($N_{\beta} = 23$) and larger ($N_{\beta} = 27$) than $N/2$ are drawn as lines on the δ - Ω plane. Note that the $N/2$ plateau lobe is centred around a value slightly larger than $\delta = 1$, which is approximately the point where the second term in equation (2) vanishes and our system becomes an effective Ising spin model.

The half filling plateau disappears with increasing Ω and we find a linear interpolation between regions with zero and full filling in this regime. This is consistent with a breakdown of the crystalline structure, and we note that in the limit $\Omega \rightarrow \infty$ for finite δ we expect the filling to be constant at $N/2$ since the state $\bigotimes_k^N (|\beta\rangle_k - |\alpha\rangle_k)/\sqrt{2}$ becomes the ground state of the system.

Note that the grid is too coarse-grained to resolve plateaus of smaller fractions of the filling. However, we observe several kinks in the particle number at small values of Ω/V_{dd} . We show below, e.g., that the feature at $\delta \approx 0.25V_{\text{dd}}$ corresponds to a crystalline state with filling $N/3$. This will verify the lobe-like structure as depicted in figure 2; however, we find that the plateau for filling $N/3$ is significantly smaller, at values of $\Omega \approx 10^{-2}V_{\text{dd}}$. For values of $\delta \sim 2.25V_{\text{dd}}$ we also observe some kinks, which correspond to regular patterns in the lattice with two subsequent sites being in the strongly interacting state, followed by one site being in the state $|\alpha\rangle_k$.

In order to illustrate the claim that the plateaus seem to belong to crystalline states, we can investigate the fluctuation in the total occupation number of the strongly interacting state,

$$\Delta N_{\beta} \equiv \sum_{k,l}^N \langle \hat{n}_k \hat{n}_l \rangle - N_{\beta}^2. \quad (4)$$

In figure 4, we show ΔN_{β} for $\delta = 1.1V_{\text{dd}}$ and $0.05V_{\text{dd}} \leq \Omega \leq 5V_{\text{dd}}$. We find that ΔN_{β} decreases significantly with decreasing Ω and crossover behaviour is centred around $\Omega \approx 0.2V_{\text{dd}}$. For $\Omega \lesssim 0.2$ a crystalline state with nearly no fluctuations $\Delta N_{\beta} \lesssim 3 \ll N = 50$ is present. For large Ω , ΔN_{β} converges to a value close to $N/4 = 12.5$, which is the correct result for finite δ and $\Omega \rightarrow \infty$, i.e. where $\bigotimes_k^N (|\beta\rangle_k - |\alpha\rangle_k)/\sqrt{2}$ becomes the exact ground state of the system. Note

that the quantity ΔN_β is related to the Mandel Q -factor $Q \equiv \Delta N_\beta / N_\beta - 1$, which has been measured in recent experiments for the number of Rydberg excitations in small ensembles of cold atoms [39] and quantifies the deviation from a Poissonian number statistic [40].

To study ground states in more detail for different parameter regimes and demonstrate clearly the crystalline behaviour, we evaluate DDC functions, defined as

$$\mathcal{G}_k^{[i]} \equiv \langle \hat{n}_i \hat{n}_{i+k} \rangle - \langle \hat{n}_i \rangle \langle \hat{n}_{i+k} \rangle. \quad (5)$$

In a finite system with open boundary conditions, the exact values of $\mathcal{G}_k^{[i]}$ will differ from site i where the DDC is evaluated. However, decay behaviour of the correlation functions for large k should be independent of the site index i in a sufficiently large system. To distinguish ground-state phases by their decay behaviour, we will first calculate ground states of a system with periodic boundary conditions, in which the DDC becomes site independent. We then drop the site index and write \mathcal{G}_k .

In figure 5(a), we show a characteristic DDC in the parameter regime where the filling of the lattice is approximately $N/2$, choosing a detuning of $\delta = 1.1 V_{\text{dd}}$, with both $\Omega = 0.1 V_{\text{dd}}$ and $\Omega = 0.2 V_{\text{dd}}$. The inset in figure 5(a) shows the modulus of the correlation function, $|\mathcal{G}_k|$, on a logarithmic scale. In the regime of the half filling plateau we indeed find a crystalline structure with a pronounced zigzag pattern. The long-range crystalline order is indicated by the decay of $|\mathcal{G}_k|$ to a non-zero value as a function of the site index k . We find that for increasing N the value of the constant to which $|\mathcal{G}_k|$ decays becomes independent of the system size.

We note, already from the comparison in figure 5(a), that as Ω / V_{dd} increases the strength of the long-range crystalline order decreases. If we continue to increase Ω / V_{dd} , we find that this order is broken entirely, as shown in figure 5(b), with the same parameters, but for Rabi frequencies $\Omega = 0.3 V_{\text{dd}}$ and $\Omega = 0.4 V_{\text{dd}}$. In these cases, we also observe peaks with periodicity 2; however, these occur only for very small values of $k \lesssim 5$. As k increases, $|\mathcal{G}_k|$ decays to zero, indicating the breakdown of the long-range order. This appears as a phase transition from crystalline order to essentially a ‘paramagnetic phase’, in which the correlations typically decay exponentially. However, we note here a special feature of the correlation functions in this parameter regime, specifically that while we have exponential decay at short distances ($k \lesssim 10$), this changes to a power-law decay at longer distances. This is most clearly seen in the results for $\Omega = 0.4 V_{\text{dd}}$ in figure 5(b). By fitting a function we find that, in this region, $|\mathcal{G}_k| \approx C/k^3$, with a constant C . This is the same power-law decay as the interaction term, consistent with similar results derived for other long-range spin models [28, 41]. Physically, the correlations initially decay exponentially due to the primary influence on a given particle being from its nearest neighbours (analogous to exponentially decaying correlations in the paramagnetic phase of an Ising model). However, once correlations arising from nearest-neighbour interactions become sufficiently small, long-distance correlations will be dominated by the effects of the direct interaction between distant particles. Thus, long-range correlations are expected to decay at large distances with the same power as the interaction [41].

We find similar behaviour for crystalline states at other densities, including occupation periodicities larger than two. When the detuning is decreased from $\delta \approx 0.5 V_{\text{dd}}$ it becomes less favourable to occupy $|\beta\rangle_k$ states in the system and therefore in the case of small Ω , crystalline phases with larger spacing between these occupations appear in order to reduce the dipole–dipole interaction energy. For example, in figure 6 we show the DDC indicating an occupation of the states $|\beta\rangle_k$ on every third site for $\Omega \sim 10^{-2} V_{\text{dd}}$ and $\delta = 0.25 V_{\text{dd}}$. To make this periodicity clearer, we present results for a system with $N = 60$ sites. As in figure 5, in figure 6

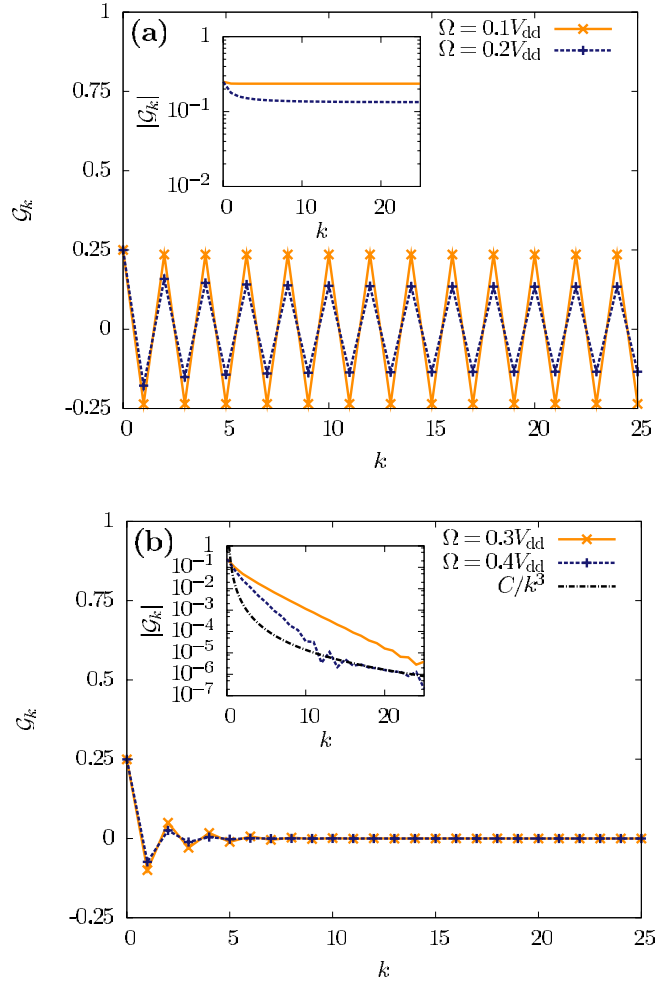


Figure 5. DDC functions \mathcal{G}_k for the ground states of Hamiltonian (1) for $\delta = 1.1V_{dd}$ and (a) $\Omega = 0.1V_{dd}$, $0.2V_{dd}$, and (b) $\Omega = 0.3V_{dd}$, $0.4V_{dd}$. The insets show the modulus $|\mathcal{G}_k|$ on a logarithmic scale. Here we show the results for a system with 50 sites and periodic boundary conditions. We find states with a marked crystalline structure of periodicity 2 in (a) and a phase transition at $0.2V_{dd} < \Omega < 0.3V_{dd}$ in terms of the decay behaviour of $|\mathcal{G}_k|$. In contrast to (a), in (b) $|\mathcal{G}_k|$ decays exponentially. In the case of $\Omega = 0.4V_{dd}$ the long-range decay behaviour ($k \gtrsim 10$) follows a power-law decay $\propto Ck^{-3}$ (with $C \approx 1.7 \times 10^{-2}$).

we observe the characteristic long-range order in the DDC, combined with a marked peak on every third lattice site. Again we find a phase transition away from crystalline order, with an exponential decay of $|\mathcal{G}_k|$ exhibited for larger values of Ω . Note that the crystalline phase with $1/3$ filling occurs in a much smaller region of parameter space than the crystalline phase with $1/2$ filling.

In what follows, we are interested in time-dependent creation of these crystalline states in the case of polar molecules or Rydberg atoms loaded into an optical lattice. These systems will typically occupy $N \sim 50$ lattice sites, with open boundary conditions generated by the unoccupied ends of the chain. Thus, rather than attempting to derive the full phase diagram

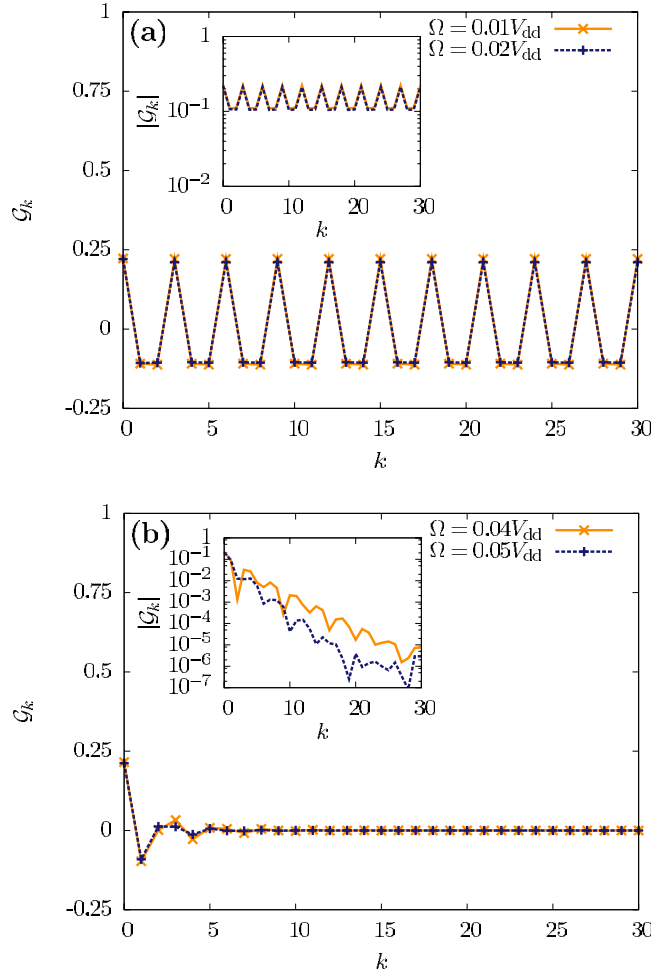


Figure 6. DDC functions \mathcal{G}_k for the ground states of Hamiltonian (1) for $\delta = 0.25V_{dd}$ and (a) $\Omega = 0.01V_{dd}$, $0.02V_{dd}$ and (b) $\Omega = 0.04V_{dd}$, $0.05V_{dd}$. The insets show the modulus $|\mathcal{G}_k|$ on a logarithmic scale. Here we show the results for a system with 60 sites and periodic boundary conditions. We find a marked crystalline structure in (a) with periodicity 3 and a phase transition at around $\Omega \approx 0.03V_{dd}$ indicated by the exponential decay behaviour of $|\mathcal{G}_k|$ in (b).

for an infinite system, we focus on the case of open boundary conditions relevant to the experiments. Although the correlation functions are modified by the boundary conditions, we show below that the characteristic signatures of different phases can still be clearly identified.

In figure 7, we show the DDC evaluated from site number 5 of an $N = 50$ site system, i.e. $\mathcal{G}_k^{[5]}$ with open boundary conditions. We choose the same parameters as were shown in figures 5(a) and (b), including crystalline phases with periodicity 2. Despite obvious effects of the open boundary conditions, we can clearly distinguish crystalline behaviour ($\Omega = 0.1V_{dd}, 0.2V_{dd}$) from the case where exponentially decaying DDCs are present ($\Omega = 0.3V_{dd}, 0.4V_{dd}$). While in the crystalline phase we find very little decay for increasing k until the effects of the boundary become apparent ($k \gtrsim 20$), in the case of $\Omega \gtrsim 0.3$ the correlations

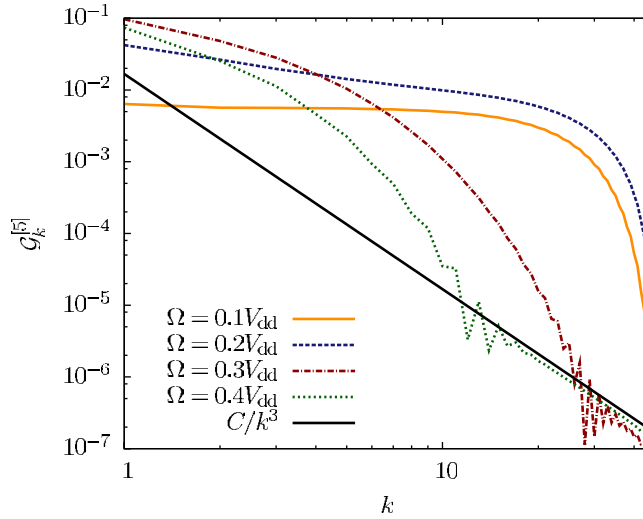


Figure 7. DDC functions evaluated from site index $i = 5$ in a 50-site system with open boundary conditions, $\mathcal{G}_k^{[5]}$. The results shown are for the same parameter regime as in figure 5. Despite strong boundary effects, a crystalline phase is still distinguishable from a phase with such a structure via the behaviour over short ranges $k \lesssim 10$. In the crystalline phase, the long-range decay follows a power-law behaviour proportional to Ck^{-3} ($C \approx 1.7 \times 10^{-2}$ is a constant).

rapidly decay below values of 10^{-5} . As in figure 5 we still observe a long-range power-law decay for $k \gtrsim 10$ proportional to k^{-3} .

In relation to figure 2, the results presented in figures 5–7 give evidence for the crystalline phases at filling factors $1/2$ and $1/3$ on the lattice, and show that for each there exist transitions as Ω is increased to non-crystalline phases. This justifies that the lobes are finite along the Ω -axis, and shows that the boundary depicted corresponds to a phase transition.

Note that the DDC functions can be measured experimentally both for Rydberg atoms and for polar molecules. Detection of these correlation functions is discussed in more detail in section 6.

5. Dynamical creation of crystalline states

5.1. Time-dependent state preparation

We now discuss the dynamical creation of crystalline states in our system. The natural initial state for the experiments corresponds to having all of the particles in the non-interacting states $|\alpha\rangle_k$, which would be the ground states for neutral atoms, or a single dressed rotational state for polar molecules. In terms of the effective model, this state is the ground state of the Hamiltonian (1) for large negative detuning and small Ω . The question now is whether one can time dependently vary the laser parameters Ω and δ , i.e. find a trajectory in the Ω - δ plane, so that this initial state is adiabatically transferred to a crystalline state of the form discussed in section 4.

In order to guide our discussion of this question, we first consider a small model system consisting of eight sites, where exact diagonalization of Hamiltonian (1) is straightforward. We

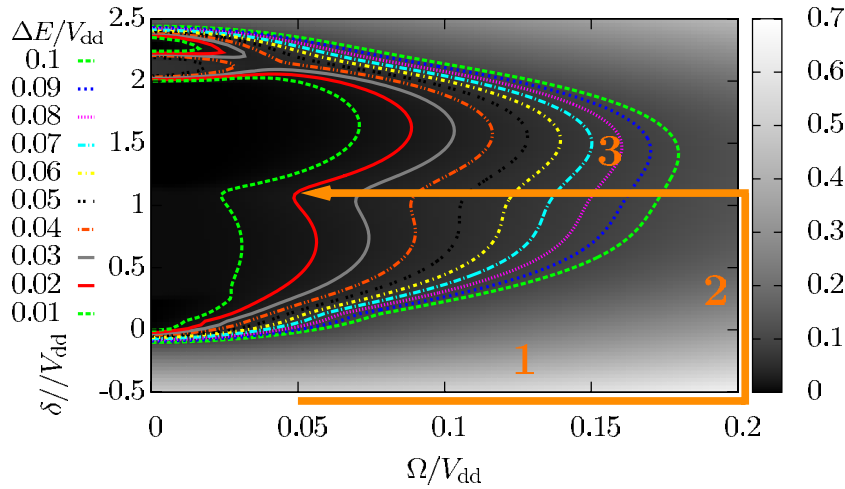


Figure 8. Shaded plot of the energy gap ΔE between the ground and the first excited state as a function of Ω and δ . The results are from exact calculations for an eight-site system with Hamiltonian (1). The lines indicate the contours of constant ΔE . A path, which consists of three segments and yields an adiabatic passage to a crystalline ground state, is sketched as an orange arrow (see text).

can then estimate possible paths for the adiabatic transfer based on the size of the energy gap ΔE between the ground state and excited states. During the adiabatic ramp, we would like ΔE to remain as large as possible to suppress non-adiabatic transitions to excited states of the effective model. In figure 8, we show a shaded plot of the energy gap between the ground state and the first excited state as a function of Ω and δ , with lines of constant energy gap marked in the plot. Close to $\Omega = 0$, we find a large region where the energy gap assumes small values and where one can recognize lobe-like structures. Lobes at values of $\delta \approx 2.25V_{dd}$ are especially visible. As mentioned before, these correspond to states with regular patterns of two subsequent sites being in the strongly interacting state. In contrast to the lobe for filling fraction $N/3$ of the strongly interacting state at $\delta \approx 0.25V_{dd}$, these are enhanced due to the larger increase in interaction energy when adding single occupations of the strongly interacting state to the system. Therefore, these lobes are more robust when increasing Ω . In general, the system is too small to observe lobes of filling fractions $N/3$ and smaller and these are only visible as small kinks for $\delta \approx 0.25V_{dd}$. With increasing Rabi frequency Ω the energy gap increases. The requirement of having at any instance of time a sufficiently large energy gap is most easily fulfilled if one chooses to ‘steer’ a path in parameter space around those regions where the gap is the smallest. A simple path that seems to achieve this is, for example, to first increase Ω at constant large negative detuning δ and then increase δ at a constant large Ω . Both steps can be achieved by changing the parameters δ and Ω rapidly, due to the large gap ΔE present at all times. Afterwards, Ω can be decreased to a small value on a line of constant δ . This path consisting of three segments is marked in figure 8 by an orange arrow.

Now we would like to test these insights by investigating the time-dependent propagation of the system along this path in parameter space. In order to investigate the scaling with the system size, we study systems of size 20, 30, 40 and 50 lattice sites. We note that the large sizes here are already typical of likely experimental setups. As an example, we choose to prepare

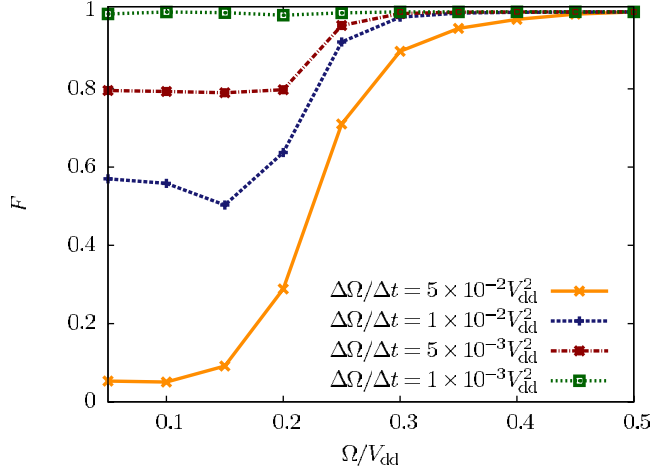


Figure 9. The fidelity of the adiabatically evolved state with the current ground state, when changing Ω from $0.50V_{\text{dd}}$ to $0.05V_{\text{dd}}$ at constant $\delta = 1.1V_{\text{dd}}$ in segment 3 of the adiabatic preparation path. Results are shown for different variation rates $\Delta\Omega/\Delta t$ within a 30-site system with Hamiltonian (1). For decreasing variation rates the final fidelity for the crystalline state (at $\Omega = 0.05V_{\text{dd}}$) increases towards 1.

a crystalline state with excitation periodicity 2, which is the ground state of our model for the parameters $\Omega = 0.05V_{\text{dd}}$ and $\delta = 1.1V_{\text{dd}}$. We perform real-time simulations for a path consisting of three segments, as sketched in figure 8. We start at $\Omega = 0.05V_{\text{dd}}$ and $\delta = -3V_{\text{dd}}$. There, the inner product between the ground state of the Hamiltonian and the state in which all atoms are in the $|\alpha\rangle_k$ state is sufficiently large for all system sizes. The segments of the path are

1. We increase Ω from $0.05V_{\text{dd}}$ to $0.5V_{\text{dd}}$ at $\delta = -3$ with a variation rate $\Delta\Omega/\Delta t = 0.05V_{\text{dd}}^2$.
2. We increase δ from $-3V_{\text{dd}}$ to $1.1V_{\text{dd}}$ at $\Omega = 0.5V_{\text{dd}}$ with a variation rate $\Delta\delta/\Delta t = 0.05V_{\text{dd}}^2$.
3. We decrease Ω from $0.5V_{\text{dd}}$ to $0.05V_{\text{dd}}$ with several variation rates $\Delta\Omega/\Delta t$.

Due to the large gaps in the energy spectrum it is possible for segments 1 and 2 to obtain states with a high fidelity $F \equiv |\langle\Psi_G(\Omega, \delta)|\Psi(t)\rangle|^2 \sim 1$ in the comparison of our evolved state, $|\Psi(t)\rangle$, with the ground state of the effective model with the corresponding parameters $|\Psi_G(\Omega, \delta)\rangle$ on that path. The most sensitive part of this process is the third segment. In figure 9, we show the fidelity F of the adiabatically evolved state along segment 3 as a function of $\Omega(t)$ and for various variation rates $\Delta\Omega/\Delta t$. On $N = 30$ lattice sites, we find that for the three rates $\Delta\Omega/\Delta t = 5 \times 10^{-2}V_{\text{dd}}$, $1 \times 10^{-2}V_{\text{dd}}$ and $5 \times 10^{-3}V_{\text{dd}}$, this fidelity drops below values of 80%, which occurs when crossing the phase transition from figure 5, i.e. in the regime $0.2V_{\text{dd}} < \Omega < 0.3V_{\text{dd}}$. At this point the ground-state gap becomes too small and excitations to higher excited states analogous to Landau–Zener tunnelling processes occur. However, when using a rate of $\Delta\Omega/\Delta t = 1 \times 10^{-3}V_{\text{dd}}$, we find that the fraction of the state that is lost into higher excitations remains reasonably small and the final fidelity with the crystalline state at $\Omega = 0.05V_{\text{dd}}$ is larger than $F \approx 99\%$. Thus, we have shown that a crystalline state can be produced with very high fidelity in a finite system of 30 sites. The timescale that is required

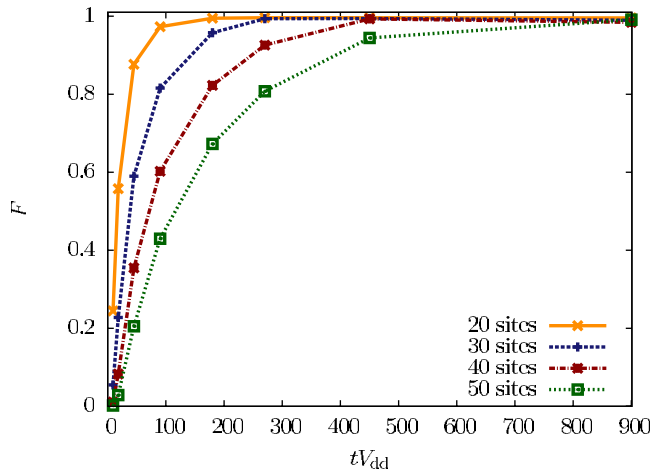


Figure 10. The fidelity of the time-evolved state with the target crystalline state, at $\Omega = 0.05 V_{\text{dd}}$, and $\delta = 1.1 V_{\text{dd}}$ as a function of time required for segment 3. Here we show results for several system sizes of 20, 30, 40 and 50 lattice sites. This fidelity decreases with increasing system size and with decreasing preparation time.

for all three segments is of the order of $500/V_{\text{dd}}$, and we will show that this is experimentally realizable for our two physical implementations below.

In an experiment with either polar molecules or neutral atoms coupled to excited Rydberg states in an optical lattice, the final state could be characterized by measuring DDC functions. These can be most easily detected directly by *in situ* imaging experiments [42]. In the case of polar molecules, the crystalline structure will be visible in noise-correlation measurements of state-selective momentum distributions of molecules released from the lattice [43]–[45]. In these correlation measurements, the periodicity of the crystalline structure would be present as a peak at the corresponding reciprocal lattice vector. In the case of Rydberg excitations, direct measurement of DDC functions could also be made by imaging the sample on a channel plate detector [20].

An important question is: To what extent can the same fidelities we have observed for a system size of 30 lattice sites also be achieved for larger system sizes? In general, we expect the energy gap between ground and excited states to become smaller with increasing system size, and we expect the measure of the fidelity to become more sensitive due to the exponentially increasing size of the Hilbert space. To analyse how much this affects the final fidelity, in figure 10 we plot the fidelity achieved after ramping the laser parameters through all segments of our preparation procedure, as a function of the time required for the final segment 3. We consider system sizes of 20, 30, 40 and 50 sites.

We find that for all system sizes the fidelity is $> 94\%$ when choosing a variation rate slower than $\Delta\Omega/\Delta t = 1 \times 10^{-3} V_{\text{dd}}^2$, which corresponds to an operation time of approximately $450/V_{\text{dd}}$ on segment 3. In the case of an even slower rate of $\Delta\Omega/\Delta t = 5 \times 10^{-4} V_{\text{dd}}^2$, which requires a time of approximately $900/V_{\text{dd}}$, the fidelity becomes larger than 98%, even in the case of a system with 50 lattice sites. This fidelity is very high, especially given that the Hilbert space dimension is 2^{50} in the latter case.

5.2. Comparison with experimental parameters

Let us compare the time required to reach this final crystalline phase with experimentally accessible timescales, which are in general limited by the finite lifetime of the strongly interacting state. In the scheme presented above, at the slowest variation rate of $\Delta\Omega/\Delta t = 5 \times 10^{-4} V_{\text{dd}}^2$ on segment 3, a total operation time of the order of $1000/V_{\text{dd}}$ is required. Note that this time can be further dramatically decreased by choosing shorter paths or by not using a constant ramping rate but rather reducing it with time while approaching the critical point of the phase transition.

In the case of the polar molecule implementation (see section 6.1 for more details), typical parameters give $V_{\text{dd}} \approx 10\hbar$ kHz, assuming a permanent dipole moment $d_0 = 1$ Debye and a lattice spacing of $a = 400$ nm. This translates to a time for the complete preparation of approximately 0.1 s, which is significantly shorter than recently measured lifetimes of molecules in an optical lattice of 8 s [46]. By choosing polar molecules with larger dipole moments like LiCs ($d_0 \approx 5.5$ Debye [24]), the preparation time can be further reduced down to the order of a few ms.

In the case of the Rydberg atom implementation (see section 6.2 for more details), if we choose a principal quantum number $n = 14$, then $V_{\text{dd}} \approx 7\hbar$ GHz (assuming a lattice spacing of $a = 400$ nm). Hence, the total operation time corresponds to approximately 140 ns in the experiment. This value is well below the typical lifetime of an $n = 14$ Rydberg level of lithium, which can be found to be approximately $2.2 \mu\text{s}$ [47]. Note that these estimates neglect the effects of blackbody radiation, which can redistribute the population among excited levels. For Rydberg atoms, in general the lifetime increases with increasing n and, furthermore, the required operation time decreases as n^{-4} . However, the disadvantage of large principal quantum numbers is the small-level distances Δ_{inter} and Δ_{intra} (see figure 13), which both decrease with n . This limits the experimentally accessible values of δ . In case $n = 14$ ($a = 400$ nm) at an electric field strength of $F_{\text{el}} = 100 \text{ kV m}^{-1}$, we can estimate by using the results known from the hydrogen atom $\Delta_{\text{inter}} \approx 4.6 \times 10^3 V_{\text{dd}}$ and $\Delta_{\text{intra}} \approx 90 V_{\text{dd}}$. The field strength is thereby well below the Inglis–Teller limit, which is in this case 319 kV m^{-1} [48]. This justifies the validity of our two-level model, derived in section 6.2, in this regime.

This comparison to the lifetime of a single Rydberg atom is oversimplified, as in the presence of N_β excited atoms, the rate of single decay events will increase roughly in proportion to N_β .⁵ However, as the system size (and hence N_β) becomes larger, the effect of a single decay on the crystalline structure should decrease. While the many-body state fidelity will be very sensitive to a single decay, DDC functions should be robust, at least on length scales smaller than those separating places where spontaneous emissions have occurred. The effect on the many-body state of single decay events also depends on when during the excitation process they occur. A full treatment of this excitation process including decay events could be achieved by studying the dynamics of a master equation including spontaneous emission events.

Therefore and from the results in figure 10, we conclude that the adiabatic passage should be experimentally realizable for both our implementations of the effective spin model with a size of ~ 50 sites. For larger system sizes, longer timescales will be required for reaching fidelities as high as those we have obtained here. However, the properties of the final states will typically be determined in an experiment by the measurement of correlation functions. In contrast to the

⁵ This neglects superradiant effects, which should be small as the excitations are separated by distances of the order of optical wavelengths [49].

state fidelity, correlation functions (together with the physical character of the state) become more robust to small non-adiabaticities (especially those resulting in localized defects) in larger systems.

6. Physical implementations of a long-range spin model

6.1. Polar molecules in an optical lattice

In the following, we describe how to implement Hamiltonian (1) with a system of polar molecules. We consider N molecules confined to the lowest motional level on subsequent sites of a deep 1D optical lattice, with modefunction $\phi_k(\mathbf{x})$ on site k . We assume that the lattice is sufficiently deep so that tunnelling between wells of the lattice is strongly suppressed on typical experimental timescales. In particular, we consider molecules in their electronic vibrational ground-state manifold with a closed shell structure $^1\Sigma$, which possess permanent dipole moments (e.g. $^{40}\text{K}^{87}\text{Rb}$ -like in recent experiments [7]). The setup is depicted in figure 1. We use a strong and a weak microwave field linearly polarized along the z -axis and an additional static field aligned along the same direction. Given the fact that we consider samples of the order of a few to 100 μm , one can neglect the spatial variation of the respective static and microwave fields along the optical lattice axis, which is aligned in the \mathbf{e}_x -direction.

The low-energy spectrum of a single molecule at site k in our setup is well described by rotational excitations, governed by a rigid rotor Hamiltonian coupled to the fields via an electric dipole interaction [50]–[53]

$$\hat{H}_{\text{rot}}^k(t) = B\hat{\mathbf{J}}_k^2 - \hat{d}_k^z (E_{\text{dc}} + E_1^z(t) + E_2^z(t)). \quad (6)$$

Here, B is the rotational constant typically of the order of tens of GHz ($\hbar \equiv 1$) [26], $\hat{\mathbf{J}}_k$ is the angular momentum operator, \hat{d}_k^z is the z -component of the dipole operator and E_{dc} , $E_1^z(t) = E_1^z \exp(-i\omega_1 t) + \text{c.c.}$ and $E_2^z(t) = E_2^z \exp(-i\omega_2 t) + \text{c.c.}$ are the static, weak and strong external microwave fields, respectively.

The eigenstates of $\hat{\mathbf{J}}_k^2$ are denoted by $|J, m_J\rangle_k$ with eigenvalues $J(J+1)$ ($\hbar \equiv 1$), and $m_J = -J, \dots, J$ being the eigenvalues of the projection onto the z -axis, \hat{J}_k^z . The dipole operator \hat{d}_k^z couples rotational states with differences $\Delta J = \pm 1$, and we recall that the eigenstates of equation (6) have no net dipole moment. The non-vanishing elements of the operator \hat{d}_k^z are given by $\langle J \pm 1, m_J | \hat{d}_k^z | J, m_J \rangle_k = d_0(J, m_J; 1, 0 | J \pm 1, m_J)(J, 0; 1, 0 | J \pm 1, 0) \sqrt{(2J+1)/(2(J \pm 1) + 1)}$ in terms of the Clebsch–Gordan coefficients $(J_1, m_1; J_2, m_2 | J, m)$, where d_0 denotes the permanent electric dipole moment along the internuclear axis, which is typically of the order of a few Debyes [23, 24].

By applying electric fields, one lifts the degeneracy of the state manifolds with $J > 0$ and induces a finite dipole moment in the dressed rotational states. Since the fields are aligned along the quantization axis, m_J is conserved, and we focus on states with $m_J = 0$ in our setup, which are connected to the ground state. The induced dipole moments of two molecules at distinct sites k and l then lead to an energy shift due to the dipole–dipole interaction potential.

In order to describe this, we need to consider many molecules on the lattice. Molecules in an internal state denoted by σ can then be represented by field operators $\hat{\Psi}_\sigma(\mathbf{x})$, obeying the standard bosonic or fermionic commutation relations. We consider a situation where no motional modes other than $\phi_k(\mathbf{x})$ for each site k are populated during the experiment, which

is valid provided that the band separation ω_T is substantially larger than the laser coupling parameters and interaction energies. Thus, we can expand the field operators as

$$\hat{\Psi}_\sigma(\mathbf{x}) = \sum_k \phi_k(\mathbf{x}) \hat{g}_k^\sigma \quad (7)$$

and identify individual molecules occupying each mode described by the operators \hat{g}_k^σ . Since all rotational states we consider here have $m_J = 0$, they are only coupled by an interaction proportional to $\hat{d}_k^z \hat{d}_l^z$, which can be integrated over the modefunctions in each lattice site. The resulting many-body Hamiltonian of a system for N molecules can be written as

$$\hat{H}_{\text{pm}}(t) \approx \sum_k^N \hat{H}_{\text{rot}}^k(t) + V_{\text{dd}}^{(1)} \sum_{k \neq l}^N \frac{\hat{d}_k^z \hat{d}_l^z}{|k-l|^3}, \quad (8)$$

with lattice spacing a , and where $V_{\text{dd}}^{(1)} \approx 1/(8\pi\epsilon_0 a^3)$. Note that we neglected corrections to the shape of the interactions, which are of the order of $\mathcal{O}(l_{\text{H}}/(a|k-l|))$, where l_{H} denotes the characteristic harmonic oscillator length for the optical potential well on each site.

A suitable choice of external electric fields then makes it possible to strongly couple/dress locally two (effective) rotational levels, such that only one level has a strong induced dipole moment, while at the same time the transition dipole moment remains negligibly small. This results in dipole–dipole interactions in equation (8) reducing to the diagonal form of equation (1).

We now detail our appropriate choice of electric fields for obtaining the desired dressed states. The key idea is to apply the static field E_{dc} for inducing a finite dipole moment in the rotational states, leading to the dressed states $|J\rangle_{\text{dc}}$, defined by $[B\hat{\mathbf{J}}_k^2 - \hat{d}_k^z E_{\text{dc}}]|J\rangle_{\text{dc}} = E_J|J\rangle_{\text{dc}}$ (see figure 11(b)), and to then couple the two states $|1\rangle_{\text{dc}}$ and $|2\rangle_{\text{dc}}$ by a strong microwave field $E_2^z(t)$, such that the dipole moment vanishes in one of the resulting dressed states. The field $E_2^z(t)$ is tuned to the transition between the two states with Rabi frequency $\Omega_2 \equiv \langle 2|\hat{d}_k^z|1\rangle_{\text{dc}} E_2^z$ and detuning $\Delta_2 \equiv \omega_2 - (E_2 - E_1)$ (see figure 11). Diagonalizing the corresponding two-level Hamiltonian and making the rotating wave approximation lead to the two dressed states $|\alpha_\pm\rangle_k = \cos(\theta/2)|1\rangle_{\text{dc}} - \sin(\theta/2)|2\rangle_{\text{dc}}$ with the dressing angle $\theta \equiv \arctan(-2\Omega_2/\Delta_2)$ ($0 < \theta < 2\pi$), where the state $|\alpha_-\rangle_k$ ($|\alpha_+\rangle_k$) corresponds to $\theta < \pi$ ($\theta > \pi$). The corresponding energies of the dressed states are $E_{\alpha^\pm} = E_1 - \Delta_2/2 \pm \sqrt{\Delta_2^2 + 4\Omega_2^2}/2$.

Finally, we couple the state $|\alpha\rangle_k \equiv |\alpha_-\rangle_k$ and the state $|\beta\rangle_k \equiv |0\rangle_{\text{dc}}$ by the weak electric field with Rabi frequency $\Omega_1 \equiv \langle \alpha|\hat{d}_k^z|\beta\rangle_k E_1^z$ and detuning $\Delta_1 \equiv \omega_1 - (E_\alpha - E_0)$. Thereby we assume that the field $E_1^z(t)$ is much weaker than $E_2^z(t)$, so that the states $|\alpha\rangle$ and $|\beta\rangle$ are unaffected by $E_1^z(t)$. Going to the rotating frame and making the rotating wave approximation the many-body Hamiltonian becomes time independent and reads

$$\hat{H}_{\text{pm}} = \Omega_1 \sum_k^N \hat{\sigma}_k^x - \Delta_1 \sum_k^N \hat{n}_k + V_{\text{dd}}^{(1)} \sum_{k \neq l}^N \frac{\hat{V}_{\text{d}}}{|k-l|^3}, \quad (9)$$

with $\hat{\sigma}_x \equiv |\beta\rangle\langle\alpha|_k + |\alpha\rangle\langle\beta|_k$ and $\hat{n}_k \equiv |\beta\rangle\langle\beta|_k$. In the last term of equation (9), \hat{V}_{d} is the dipole–dipole interaction matrix in the rotating frame, which in the two-molecule basis

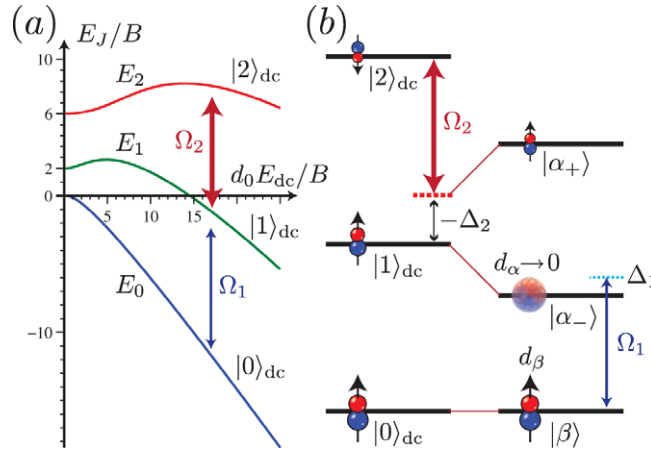


Figure 11. Level scheme for a system of polar molecules in a combination of static and microwave fields, cf figure 1. (a) Energy levels E_J of a molecule in a static electric field E_{dc} . The field orients the dipoles, i.e. induces finite permanent dipole moments in each rotational state $|J\rangle_{dc}$. (b) A strong linearly polarized microwave field $E_2^z(t)$ couples the states $|1\rangle_{dc}$ and $|2\rangle_{dc}$ with the Rabi frequency Ω_2 and detuning Δ_2 . Fine-tuning the microwave field (with respect to the static field) makes it possible to cancel the permanent dipole moment in one of two dressed states, $|\alpha_+\rangle$ and $|\alpha_-\rangle$, cf $d_\alpha \rightarrow 0$. A second (weaker) microwave field $E_1^z(t)$ finally couples the ground state $|\beta\rangle \equiv |0\rangle_{dc}$ to the dressed state with vanishing dipole $|\alpha\rangle$ with an effective Rabi frequency Ω_1 and detuning Δ_1 .

$\{|\alpha\rangle_k|\alpha\rangle_l, |\alpha\rangle_k|\beta\rangle_l, |\beta\rangle_k|\alpha\rangle_l, |\beta\rangle_k|\beta\rangle_l\}$ is

$$\hat{V}_d \equiv \begin{pmatrix} d_\alpha^2 & 0 & 0 & 0 \\ 0 & d_\alpha d_\beta & d_{\beta\alpha}^2 & 0 \\ 0 & d_{\beta\alpha}^2 & d_\alpha d_\beta & 0 \\ 0 & 0 & 0 & d_\beta^2 \end{pmatrix} \quad (10)$$

Here, $d_\alpha \equiv \langle \alpha | \hat{d}_k^z | \alpha \rangle_k$, $d_\beta \equiv \langle \beta | \hat{d}_k^z | \beta \rangle_k$ and $d_{\beta\alpha} \equiv \langle \beta | \hat{d}_k^z | \alpha \rangle_k$ are the dressed single-particle dipole operator elements.

Our goal is to find values of the microwave dressing angle θ and of the static field strength E_{dc} , for which the permanent dipole moment d_α and the transition dipole moment $d_{\beta\alpha}$ become negligible compared to the permanent dipole moment d_β . Then the only remaining entry in equation (10) is d_β^2 , such that a dipole–dipole interaction is only present if both molecules are in the strongly interacting state $|\beta\rangle_k$.

To this purpose, we compute the respective values of d_α , $d_{\beta\alpha}$ and d_β as a function of the microwave field angle θ and the electric field strengths up to $E_{dc} = 25d_0/B$. Figure 12 summarizes our results. In particular, in figure 12(a) (figure 12(b)) we show the ratio of the permanent dipole moments in the two states, d_α/d_β (the ratio of the transition dipole moments $d_{\beta\alpha}/d_\beta$), as a function of $E_{dc} = 25d_0/B$ and θ . The solid lines show contours of constant ratio. For both ratios, we find a distinct set of optimal parameters (E_{dc}, θ) , where one obtains a vanishing (a) permanent dipole moment d_α and (b) transition dipole moment d_β (thick black

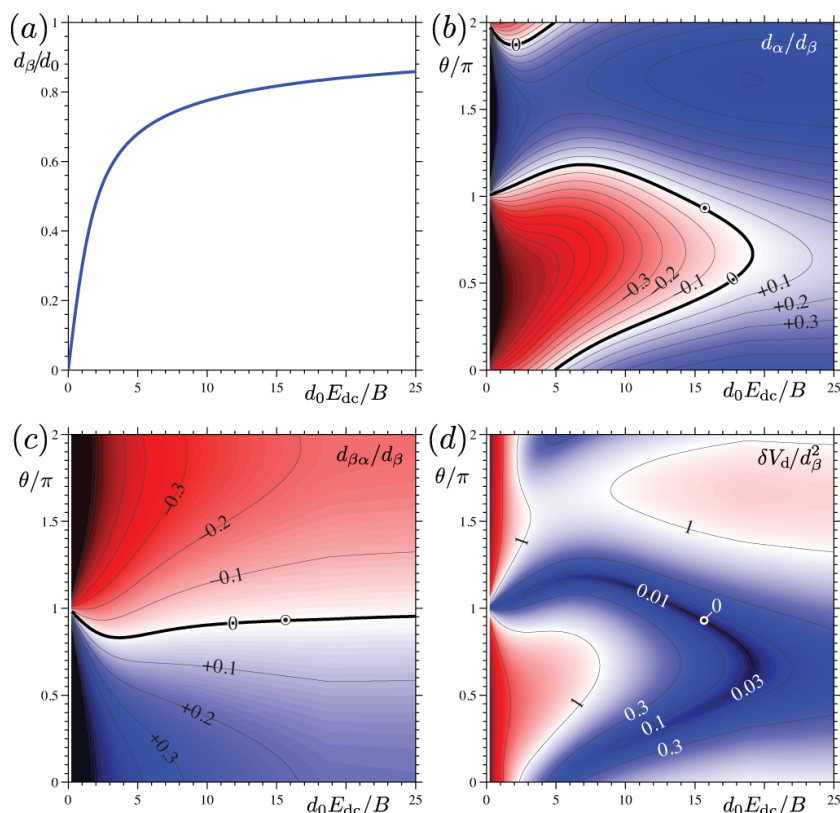


Figure 12. Effective dipole moments of a molecule in a combination of static and microwave fields, E_{dc} and $E_2^z(t)$. (a) The dipole moment d_β (in units of d_0) induced by the static electric field. (b) The ratio d_α/d_β of the two permanent dipole moments and (c) the ratio $d_{\beta\alpha}/d_\beta$ of the transition to permanent dipole moment as a function of the static-field strength $d_0 E_{dc}/B$ and the microwave-dressing angle θ . (d) The relative deviation, $\delta V_d/d_\beta^2$, of the induced dipole–dipole coupling with respect to the model interaction (1) as a function of $d_0 E_{dc}/B$ and θ . The thick solid lines show the contours of (b) vanishing dipole moment d_α and (c) vanishing transition dipole moment $d_{\beta\alpha}$. The white circle indicates the point for which one has vanishing deviations, i.e. one obtains an exact implementation of the effective model.

solid lines). We note that the two respective contour lines intersect at a specific parameter pair ($E_{dc}^\circ \approx 15.65B/d_0$, $\theta^\circ \approx 0.93\pi$) (white circle). For these parameters one obtains an exact implementation of model (1).

To quantify a deviation from an exact implementation of Hamiltonian (1) for general parameters (E_{dc}, θ) \neq ($E_{dc}^\circ, \theta^\circ$), in figure 12(c) we plot the (normalized) deviation from the model, $\delta V_d/d_\beta^2$, given by

$$\delta V_d \equiv \|\hat{V}_d - d_\beta^2 |\beta\rangle_k \langle\beta|_l \langle\beta|_k \langle\beta|_l\| = \sqrt{d_\alpha^4 + 2d_{\beta\alpha}^4 + 2d_\alpha^2 d_\beta^2}. \quad (11)$$

Since the transition dipole moment enters only quadratically into the last expression, we note that the error around the optimal point closely resembles the contour line of vanishing d_α in figure 12(a). Moreover, we find that within a range of field strength $11 \lesssim E_{dc} \lesssim 20$,

fine-tuning the microwave field allows us to obtain deviations $\delta V_d \lesssim 10^{-2} d_\beta^2$, while the permanent dipole moment $d_\beta \approx 0.8 d_0$. Thus, to a good approximation, we obtain the model interaction with a typical timescale of $V_{dd} \equiv 2d_\beta^2 V_{dd}^{(1)} \approx d_\beta^2 / 4\pi \epsilon_0 a^3 \approx 10 \hbar$ kHz for typical parameters ($a = 400$ nm, $d_\beta = 0.8$ Debye).

6.2. Neutral atoms coupled to Rydberg states

In this section, we show how to implement spin Hamiltonian (1) by making use of neutral atoms coupled to excited Rydberg states. We consider alkali atoms confined in an optical lattice in a single tube, with inter-site distance a oriented along the x -direction. Perpendicular to the lattice a homogeneous electric field, $\mathbf{F} = F_{el} \mathbf{e}_z$, is applied, together with a laser that couples the ground state $|g\rangle$ of each atom to a specific chosen Rydberg–Stark state.

6.2.1. Dipole–dipole interaction. While the atomic ground state is only slightly shifted by the external electric field, the level structure of high-lying Rydberg states is strongly altered compared to the field-free case. Nevertheless, the azimuthal symmetry of the atomic Hamiltonian is preserved such that m (the quantum number of the z -component of the electronic orbital angular momentum L_z) remains a good quantum number [48]. States with large quantum defect, i.e. usually s - and p -states, sustain a second-order Stark shift, while the degenerate states with higher angular momentum exhibit a linear Stark effect, reminiscent of the hydrogen atom [54]. The derivative of the energy with respect to the electric field strength directly yields the electric dipole moment of the given state. While the precise level structure, and therefore the dipole moment of the Stark states, depends on the element under consideration, the exact results known from the hydrogen atom usually provide good estimates for the quantities of interest.

A sketch of a Rydberg–Stark level structure is shown in figure 13. For sufficiently small field strengths, i.e. below the Inglis–Teller limit where the atom becomes ionized, the levels are grouped in manifolds, which can be labelled by the principal quantum number n . In this study, we focus on the energetically highest state of such a manifold whose azimuthal quantum number is $m = 0$. Employing the formula for hydrogen, the electric dipole moment of this state, which we denote as $|d_n\rangle$, evaluates to

$$\mathbf{d}_n = d_n \mathbf{e}_z = \frac{3}{2} e a_0 n(n-1) \mathbf{e}_z, \quad (12)$$

with e and a_0 being the charge of the electron and the Bohr radius, respectively.

Two atoms excited to the states $|d_n\rangle_k$ and $|d_n\rangle_l$ at distinct sites of the lattices k and l are expected to interact strongly via the dipole–dipole interaction potential, as already for $n = 17$ equation (12) gives a dipole moment of more than 1 kiloDebye. We intend to work in a regime in which the interaction can be treated within first-order perturbation carried out in single-particle product states. To this end it is important to note that the dipole–dipole interaction commutes with $L_{z_1} + L_{z_2}$ and therefore only couples atomic pair states for which the azimuthal quantum numbers obey $m_1 + m_2 = m'_1 + m'_2$ [8]. We assume that all these couplings are far off-resonant, which can be ensured by properly tuning Δ_{intra} and Δ_{inter} using the electric field. Moreover, accidental resonances can be avoided by restricting oneself to low principal quantum numbers n since here the two-particle energy spectrum possesses large gaps that make near-resonant

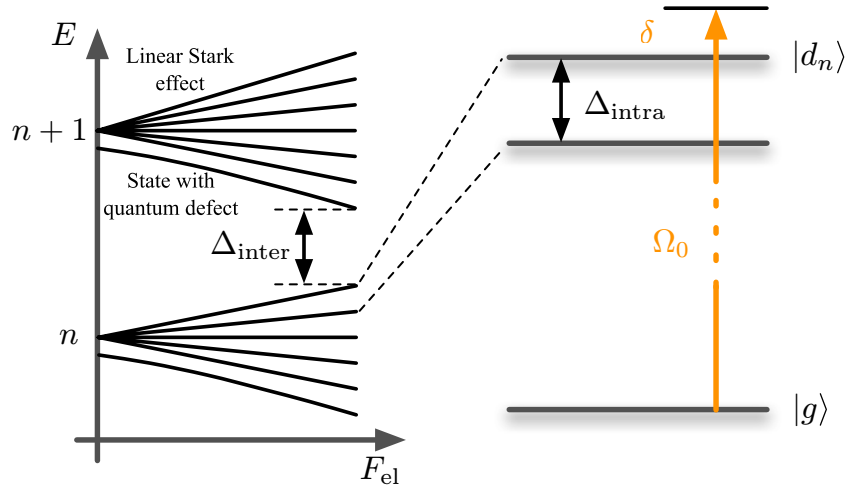


Figure 13. Sketch of the level structure of an alkali metal atom as a function of the electric field strength. The energy of hydrogen-like states grows linearly with the field strength F_{el} . Low angular momentum states with quantum defect exhibit a second-order Stark effect. In our scheme, we couple the ground state $|g\rangle$ of an atom to the Rydberg state $|d_n\rangle$, which exhibits the strongest Stark shift within the given n -manifold. The magnetic field strength and the laser parameters are set such that $\Delta_{\text{intra}} \lesssim \Delta_{\text{inter}}$, $\Delta_{\text{intra}} \gg |\delta|$ and $\Delta_{\text{intra}} \gg \Omega_0$.

excitations unlikely. Employing $\mathbf{d}_n \perp \mathbf{e}_x$, the interaction Hamiltonian between two atoms being in the product state $|d_n\rangle_k |d_n\rangle_l$ can then be written as

$$\hat{H}_{kl}^{\text{int}} = 2V_{\text{dd}}^{(1)} \frac{d_n^2}{|k-l|^3} |d_n\rangle_k |d_n\rangle_l \langle d_n|_k \langle d_n|_l, \quad (13)$$

with $V_{\text{dd}}^{(1)} \approx 1/(8\pi\epsilon_0 a^3)$, when the confinement length in each lattice site is much smaller than the lattice spacing.

We now turn to the description of the interaction between the laser and the atom. We employ a two-level approximation assuming that the ground state $|g\rangle_k$ is coupled only to the state $|d_n\rangle_k$. This is justified as long as the modulus of the laser detuning δ and the Rabi frequency Ω_0 are much smaller than the energy gaps Δ_{intra} and Δ_{inter} . Making the rotating wave approximation, the interaction of the laser with an atom located on the k th site can be written as ($\hbar = 1$)

$$\hat{H}_k^{\text{L}} = \Omega_0 (|d_n\rangle_k \langle g|_k + |g\rangle_k \langle d_n|_k) - \delta |d_n\rangle_k \langle d_n|_k \quad (14)$$

with Ω_0 and δ being the Rabi frequency and the detuning, respectively.

6.2.2. Many-body model. We now consider the many-body physics when many atoms in an optical lattice are simultaneously coupled to the state $|d_n\rangle_k$. We assume that either atoms are loaded into an optical lattice with tight radial confinement, so that we have one atom per site along a 1D tube or that we have weak radial confinement and many atoms per site. In each case, we can assume that the ground-state atoms are confined to a single modefunction at each given lattice site, $\phi_k(\mathbf{x})$. In the case of a single atom per site, this is the Wannier function for the

lowest Bloch band, and in the case of many (weakly interacting) atoms it is the solution to the Gross–Pitaevskii equation in the mean-field limit.

In order to formulate the Hamiltonian of the many-body system, we introduce field operators $\hat{\Psi}_g(\mathbf{x})$ and $\hat{\Psi}_r(\mathbf{x})$, corresponding respectively to atoms in the ground and Rydberg states, and obeying the standard bosonic (or fermionic) commutation relations. We assume that the timescale for excitation to the Rydberg state is much shorter than timescales corresponding to the atomic motion and that therefore we can neglect population of any mode function other than the $\phi_k(\mathbf{x})$ for either the ground or Rydberg states. In this case, we can approximately expand the field operators in terms of mode operators corresponding to each of these modes,

$$\hat{\Psi}_g(\mathbf{x}) = \sum_k \phi_k(\mathbf{x}) \hat{g}_k, \quad (15)$$

$$\hat{\Psi}_r(\mathbf{x}) = \sum_k \phi_k(\mathbf{x}) \hat{r}_k, \quad (16)$$

where both the initial field operators and the mode operators, \hat{g}_k^\dagger and \hat{r}_k^\dagger , obey the appropriate bosonic commutation or fermionic anti-commutation relations, depending on which atoms are used in the experiment. We can then write the Hamiltonian for a lattice with N sites as

$$\hat{H}_N \approx \Omega_0 \sum_k \left[\hat{g}_k \hat{r}_k^\dagger + \hat{g}_k^\dagger \hat{r}_k \right] - \delta \sum_k \hat{n}_k + \sum_k V_{\text{dd}}^{\text{on}} \hat{n}_k (\hat{n}_k - 1) + \frac{V_{\text{dd}}}{2} \sum_{k \neq l} \frac{\hat{n}_k \hat{n}_l}{|k - l|^3} \quad (17)$$

with $\hat{n}_k = \hat{r}_k^\dagger \hat{r}_k$ and $V_{\text{dd}} \approx d_n^2 / 4\pi\epsilon_0 a^3$. In the last term, we have again neglected corrections to the shape of the interaction potential, which are of the order of $\mathcal{O}(l_{\text{H}} / (a|k - l|))$, with l_{H} being the characteristic harmonic oscillator length for the deep optical potential well on each site.

The quantity $V_{\text{dd}}^{\text{on}}$ is relevant only in the case when we initially have many atoms per site and gives the energy offset due to the dipole–dipole interaction if two Rydberg atoms are excited on the same site. We will assume that $V_{\text{dd}}^{\text{on}} \gg V_{\text{dd}} / |k - l|^3$ for $k \neq l$ and $\Omega_0, (N\delta) \ll V_{\text{dd}}^{\text{on}}$, so that the occupation of a single site by two Rydberg atoms is far off-resonant and therefore the excitation of such a state is highly improbable. This phenomenon, which is known as the Rydberg blockade, makes it possible to restrict the maximum number of Rydberg atoms per site to 1, such that \hat{n}_k can only assume the two eigenvalues 0 and 1.

Secondly, to arrive at a Hamiltonian governing solely the dynamics of the Rydberg excitations, we eliminate the creation and annihilation operators \hat{g}_k^\dagger and \hat{g}_k in equation (17). In the case where we have an initial ground state with a single atom per site, this is simply a relabelling of the state with a single ground state atom per site as the vacuum state of the operators r_k . In the case where the mode function at each site is occupied by the same macroscopic number $N_g \gg 1$, on the other hand, we make the replacement $\hat{g}_k, \hat{g}_k^\dagger \rightarrow \sqrt{N_g}$, in which case we define the effective Rabi frequency as $\Omega = \Omega_0 \sqrt{N_g}$. The model we derive is exact under the stated assumptions when we have a fixed number of atoms per site (e.g. beginning deep in the Mott insulator regime for bosons or in a band insulator for fermions), which is the ideal experimental realization. An approximation to the model can also be obtained in a weakly interacting gas, but with some inhomogeneity in Ω for different lattice sites, both due to position dependence of the mean density (due to a trapping potential) and due to number fluctuations

between sites. In the production of crystalline states via the adiabatic ramping process discussed below, we expect that the ramp is somewhat robust against these fluctuations, especially for high filling factor crystalline states. However, this depends on the details of the realization and the inhomogeneity in Ω .

Thus, we arrive at the spin Hamiltonian describing the excitation of Rydberg states,

$$\hat{H}_{\text{ryd}} = \Omega \sum_k^N \hat{\sigma}_k^x + \delta \sum_k^N \hat{n}_k + \frac{V_{\text{dd}}}{2} \sum_{k \neq l}^N \frac{\hat{n}_k \hat{n}_l}{|k-l|^3}, \quad (18)$$

where the Pauli matrix $\hat{\sigma}_k^x \equiv \hat{r}_k^\dagger + \hat{r}_k$ has been defined. This Hamiltonian is equivalent to our model system from equation (1), with the states corresponding to $|\alpha\rangle_k \equiv |g\rangle_k$ and $|\beta\rangle_k \equiv |d_n\rangle_k$.

The scheme presented in section 5 achieves a crystalline phase of Rydberg excitations on very short timescales. However, while the preparation can be very fast compared to the lifetime of the Rydberg states, this lifetime will pose an ultimate limit to the stability of the many-body state that is produced. One way around this is to transfer the excited Rydberg states to alternative stable ground states. However, an important issue arises in this case because of the momentum kicks that arise due to the interactions between excited atoms, which can create very significant excitations in the motional states of the atoms. This is especially an issue towards the end of the chain, where the atoms will experience a force primarily in the direction away from the centre of the chain. These kicks can be estimated classically from the force acting due to the dipole–dipole interaction potential between excited Rydberg states. For crystalline states one can estimate that the net momentum kick during the crystal preparation time decreases as $k_R \propto 1/(fi)^4$, where i denotes the i th excited Rydberg atom from the boundary and f the periodicity of the crystal, i.e. with N/f filling. Quantitatively, transitions to higher bound states are given by the size of matrix elements $\int w_n(x)w_0(x)e^{ik_R x} dx$, where w_n ($n > 0$) denotes the higher band Wannier modefunctions. Thus the transition effects become small in the case when $k_R a_0$, where a_0 denotes the oscillator length, is small. The oscillator length is typically of the order of tens of nm and we can estimate the momentum kick of the boundary excitation for an $N/2$ filling crystal as roughly 1 nm^{-1} . Thus, this will be a problem for atoms at the end of the chain in the $N/2$ case, but decreases rapidly for atoms away from the edge, or a larger periodicity in the crystal. One way to circumvent this problem for the case where all lattice sites are singly occupied would be to use induced dipoles rather than direct coupling to Rydberg levels from the outset, as discussed in [55]. The idea is to make use of two stable ground states, one of which is coupled off-resonantly to a Rydberg level, producing an induced dipole with a strength depending on the parameters of the coupling and the static dipole of the Rydberg level. In this way, the coupling between ground and Rydberg states in our model is replaced by the coupling between two stable ground states. This can be achieved, e.g., via a two-photon transition. This results in much smaller values of Ω and δ (and hence also the interaction strength between excited atoms), which could even be made comparable to or less than the band gap in the optical lattice. One disadvantage of this method would be substantially increased times for the total adiabatic process; however, the ratio of the preparation time to spontaneous emission lifetime of the state could always be made large.

This method would have the added benefit of a much smaller linewidth of the coupling field for the transition between interacting and non-interacting states. In particular, for crystal periodicities other than two lattice sites, the narrow regions of detuning δ/V_{dd} for which the phases are found implies a strong condition on the stability of the laser detuning in an

experiment (and hence on the linewidth of the exciting laser). For example, a crystalline state with an excitation on every fourth site can be found in the region of $\Omega/V_{\text{dd}} = 4 \times 10^{-3}$ for $0.06 < \delta/V_{\text{dd}} < 0.09$. Using $V_{\text{dd}} \approx 7\hbar$ GHz from the previous example, this means that the range of detuning values in which states of the character are found is approximately 200 MHz, and we require that the laser linewidth be smaller than this value. This is realistic; however, for crystalline phases with even larger spacings between the excitations, the requirements become even stronger. If we use dressed dipoles, then we would be using a two-photon transition to couple between the states, for which the detuning can be controlled very accurately.

7. Conclusion and outlook

In conclusion, using adiabatic sweeps of microwave or laser parameters, it is possible to form crystalline phases of strongly interacting states in either polar molecules or neutral atoms coupled to Rydberg states in an optical lattice. The effective model Hamiltonian exhibits a rich ground-state phase diagram, with the crystalline order being destroyed as the coupling between states is increased. For typical experimental size scales and parameters we showed that preparation of crystalline structures can be achieved on reasonable timescales, and the structures can be detected by measurement of characteristic DDC functions.

The results we have obtained here motivate further study of the phase diagram with its lobe-like structure of different crystalline phases (as indicated in figure 8). This also opens the opportunity to extend 1D time-dependent simulations to the study of crystal formation in regimes of significantly larger spacing than is studied here (e.g. using matrix product operator methods [29, 30], [36]–[38]) and also to probe time-dependent transitions between the different phases. This will also allow connections to ongoing work in which the Rydberg excitations of randomly distributed atoms are being studied [20].

Acknowledgments

We thank Hans Peter Büchler, Ignacio Cirac, Markus Müller, Beatriz Olmos Sanchez, Thomas Pohl, Hendrik Weimer and Peter Zoller for helpful discussions. This work was supported by the Austrian Science Fund (FWF) through SFB FOQUS and I118_N16 (EuroQUAM_DQS) projects, by the DARPA OLE programme, by the Austrian Ministry of Science BWF, as part of the UniInfrastrukturprogramm (of the Forschungsplattform Scientific Computing and of the Centre for Quantum Physics at LFU Innsbruck), and by AFOSR MURI, EOARD grant number FA8655-10-1-308.

References

- [1] Raitzsch U, Bendkowsky V, Heidemann R, Butscher B, Löw R and Pfau T 2008 *Phys. Rev. Lett.* **100** 013002
- [2] Reetz-Lamour M, Amthor T, Deiglmayr J and Weidemüller M 2008 *Phys. Rev. Lett.* **100** 253001
- [3] Van Ditzhuijzen C S E, Koenderink A F, Hernandez J V, Robicheaux F, Noordam L D and Van Linden van den Heuvell H B 2008 *Phys. Rev. Lett.* **100** 243201
- [4] Johnson T A, Urban E, Henage T, Isenhower L, Yavuz D D, Walker T G and Saffman M 2008 *Phys. Rev. Lett.* **100** 113003
- [5] Vogt T, Viteau M, Chotia A, Zhao J, Comparat D and Pillet P 2007 *Phys. Rev. Lett.* **99** 073002

- [6] Tong D, Farooqi S M, Stanojevic J, Krishnan S, Zhang Y P, Côté R, Eyler E E and Gould P L 2004 *Phys. Rev. Lett.* **93** 063001
- [7] Ni K-K, Ospelkaus S, De Miranda M H G, Péér A, Neyenhuis B, Zirbel J J, Kotochigova S, Julienne P S, Jin D S and Ye J 2008 *Science* **322** 231
- [8] Jaksch D, Cirac J I, Zoller P, Rolston S L, Côté R and Lukin M D 2000 *Phys. Rev. Lett.* **85** 2208
- [9] Lukin M D, Fleischhauer M, Côté R, Duan L M, Jaksch D, Cirac J I and Zoller P 2001 *Phys. Rev. Lett.* **87** 037901
- [10] Urban E, Johnson T A, Henage T, Isenhower L, Yavuz D D, Walker T G and Saffman M 2009 *Nature Phys.* **5** 110
- [11] Gaëtan A, Miroshnychenko Y, Wilk T, Chotia A, Viteau M, Comparat D, Pillet P, Browaeys A and Grangier P 2009 *Nature Phys.* **5** 115
- [12] Müller M, Lesanovsky I, Weimer H, Büchler H P and Zoller P 2009 *Phys. Rev. Lett.* **102** 170502
- [13] Saffman M and Molmer K 2009 *Phys. Rev. Lett.* **102** 240502
- [14] Sun B and Robicheaux F 2008 *New J. Phys.* **10** 045032
- [15] Olmos B, Gonzalez-Ferez R and Lesanovsky I 2009 *Phys. Rev. A* **79** 043419
- [16] Olmos B, Müller M and Lesanovsky I 2010 *New J. Phys.* **12** 013024
- [17] Weimer H, Löw R, Pfau T and Büchler H P 2008 *Phys. Rev. Lett.* **101** 250601
- [18] Löw R, Weimer H, Krohn U, Heidemann R, Bendkowsky V, Butscher B, Büchler H P and Pfau T 2009 *Phys. Rev. A* **80** 033422
- [19] Olmos B, Gonzalez-Ferez R and Lesanovsky I 2009 *Phys. Rev. Lett.* **103** 185302
- [20] Pohl T, Demler E and Lukin M D 2010 *Phys. Rev. Lett.* **104** 043002
- [21] Vidal G 2003 *Phys. Rev. Lett.* **91** 147902
- [22] Vidal G 2004 *Phys. Rev. Lett.* **93** 040502
- [23] KREMS R V, STWALLEY W C and FRIEDRICH B 2009 *Cold Molecules: Theory, Experiment, Applications* (Boca Raton, FL: CRC Press)
- [24] Carr L D, DeMille D, KREMS R V and YE J 2009 *New J. Phys.* **11** 055049
- [25] Jaksch D, Venturi V, Cirac J I, Williams C J and Zoller P 2002 *Phys. Rev. Lett.* **89** 040402
- [26] *Diatom Spectral Database* <http://physics.nist.gov/PhysRefData/MolSpec/Diatom/>
- [27] Abramowitz M and Stegun I A 1965 *Handbook of Mathematical Functions with Formulas, Graphs, and Mathematical Tables* (New York: Dover)
- [28] Deng X-L, Porras D and Cirac J I 2005 *Phys. Rev. A* **72** 063407
- [29] Verstraete F, Garca-Ripoll J J and Cirac J I 2004 *Phys. Rev. Lett.* **93** 207204
- [30] Zwolak M and Vidal G 2004 *Phys. Rev. Lett.* **93** 207205
- [31] Daley A J, Taylor J M, Diehl S, Baranov M and Zoller P 2009 *Phys. Rev. Lett.* **102** 040402
- [32] Daley A J, Kollath C, Schollwöck U and Vidal G 2004 *J. Stat. Mech.* P04005
- [33] White S R and Feiguin A E 2004 *Phys. Rev. Lett.* **93** 076401
- [34] Verstraete F, Murg V and Cirac J I 2008 *Adv. Phys.* **57** 143
- [35] Gobert D, Kollath C, Schollwöck U and Schutz G 2005 *Phys. Rev. E* **71** 036102
- [36] McCulloch I P 2007 *J. Stat. Mech.* P10014
- [37] Crosswhite G M, Doherty A C and Vidal G 2008 *Phys. Rev. B* **78** 035116
- [38] Pirvu B, Murg V, Cirac J I and Verstraete F 2010 *New J. Phys.* **12** 025012
- [39] Cubel Liebisch T, Reinhard A, Berman P R and Raithel G 2005 *Phys. Rev. Lett.* **95** 253002
- [40] Ates C, Pohl T, Pattard T and Rost J M 2006 *J. Phys. B: At. Mol. Opt. Phys.* **39** 11 L233–9
- [41] Schuch N, Cirac J I and Wolf M M 2006 *Commun. Math. Phys.* **267** 65
- [42] Bakr W S, Gillen J I, Peng A, Fölling S and Greiner M 2009 *Nature* **462** 74–7
- [43] Altmann E, Demler E and Lukin M D 2004 *Phys. Rev. A* **70** 013603
- [44] Fölling S, Gerbier F, Widera A, Mandel O, Gericke T and Bloch I 2005 *Nature* **434** 481–4
- [45] Greiner M, Regal C A, Stewart J T and Jin D S 2005 *Phys. Rev. Lett.* **94** 110401
- [46] Danzl J G, Mark M J, Haller E, Gustavsson M, Hart R, Aldegunde J, Hutson J M and Nägerl H C 2010 *Nature Phys.* **6** 265–70

- [47] Theodosiou C E 1984 *Phys. Rev. A* **30** 2881
- [48] Gallagher T F 1994 *Rydberg Atoms* (Cambridge: Cambridge University Press)
- [49] Saffman M, Walker T G and Molmer K 2010 *Rev. Mod. Phys.* **82** 2313–63
- [50] Büchler H P, Demler E, Lukin M D, Micheli A, Prokof'ev N, Pupillo G and Zoller P 2007 *Phys. Rev. Lett.* **98** 060404
- [51] Micheli A, Pupillo G, Büchler H P and Zoller P 2007 *Phys. Rev. A* **76** 043604
- [52] Herzberg G 1950 *Molecular Spectra and Molecular Structure. I: Spectra of Diatomic Molecules* (New York: Van Nostrand Reinhold)
- [53] Brown J M and Carrington A 2003 *Rotational Spectroscopy of Diatomic Molecules* (Cambridge: Cambridge University Press)
- [54] Zimmermann M L, Littmann M G, Kash M K and Kleppner D 1979 *Phys. Rev. A* **20** 2251
- [55] Pupillo G, Micheli A, Boninsegni M, Lesanovsky I and Zoller P 2010 *Phys. Rev. Lett.* **104** 223002